Meox2/Tcf15 Heterodimers Program the Heart Capillary Endothelium for Cardiac Fatty Acid Uptake

Giulia Coppiello, PhD; Maria Collantes, PhD; María Salomé Sirerol-Piquer, PhD;
Sara Vandenwijngaert, PhD; Sandra Schoors, MSc; Melissa Swinnen, PhD;
Ine Vandersmissen, MSc; Paul Herijgers, MD, PhD; Baki Topal, MD, PhD;
Johannes van Loon, MD, PhD; Jan Goffin, MD, PhD; Felipe Prósper, MD, PhD;
Peter Carmeliet, MD, PhD; Jose Manuel García-Verdugo, MD, PhD; Stefan Janssens, MD, PhD;
Iván Peñuelas, PhD; Xabier L. Aranguren, PhD*; Aernout Luttun, PhD*

Background—Microvascular endothelium in different organs is specialized to fulfill the particular needs of parenchymal cells. However, specific information about heart capillary endothelial cells (ECs) is lacking.

Methods and Results—Using microarray profiling on freshly isolated ECs from heart, brain, and liver, we revealed a genetic signature for microvascular heart ECs and identified Meox2/Tcf15 heterodimers as novel transcriptional determinants. This signature was largely shared with skeletal muscle and adipose tissue endothelium and was enriched in genes encoding fatty acid (FA) transport–related proteins. Using gain- and loss-of-function approaches, we showed that Meox2/Tcf15 mediate FA uptake in heart ECs, in part, by driving endothelial CD36 and lipoprotein lipase expression and facilitate FA transport across heart ECs. Combined *Meox2* and *Tcf15* haplodeficiency impaired FA uptake in heart ECs and reduced FA transfer to cardiomyocytes. In the long term, this combined haplodeficiency resulted in impaired cardiac contractility.

Conclusions—Our findings highlight a regulatory role for ECs in FA transfer to the heart parenchyma and unveil 2 of its intrinsic regulators. Our insights could be used to develop new strategies based on endothelial Meox2/Tcf15 targeting to modulate FA transfer to the heart and remedy cardiac dysfunction resulting from altered energy substrate usage. (***Circulation***. 2015;131:815-826. DOI: 10.1161/CIRCULATIONAHA.114.013721.)

Key Words: endothelium ■ fatty acids ■ heart ■ metabolism ■ transcription factors

Endothelial cells (ECs) lining capillaries of different organs have specialized gene expression patterns, morphologies, and functions related to the specific needs of tissue parenchymal cells with which they communicate.[1] This heterogeneity is determined by environmental cues and intrinsic regulators (eg, transcription factors or TFs), which remain largely unknown.[1] Although specific characteristics of capillary ECs have been described for liver[2] and brain,[3] such information for heart ECs is lacking, with the exception of their documented modulating role in myocardial contractile performance.[4,5] As a continuously contracting organ, the heart daily produces ≈20 times its own weight in adenosine triphosphate (ATP). Mainly glucose and fatty acids (FAs) serve as substrates for ATP production. Under physiological conditions, FAs account for 60% to 90% of ATP generation, whereas glucose contributes for 10% to 40%.[6] A broad range of cardiomyopathies leading to cardiac hypertrophy and failure are associated with chronic alterations in cardiac energy metabolism, in general, and FA use, in particular.[6–12] Besides the demonstrated role of molecules involved in FA metabolism in cardiomyocytes, recent findings suggest that proteins involved in FA uptake and transport in ECs

Clinical Perspective on p 826

and cardiomyocytes may also play a role in these pathologies.[13–21] Nevertheless, it has not been established whether cardiac ECs are specialized to fulfill the high FA delivery demanded by the heart.

Recent studies identified vascular endothelial growth factor (VEGF)-B as a paracrine mediator of FA uptake through ECs in the heart, brown adipose tissue, and skeletal muscle and showed that VEGF-B inhibition protected against type 2 diabetes mellitus by decreasing FA uptake and reverting muscle metabolism toward glucose consumption.[21,22] However, EC-intrinsic (transcriptional) regulators determining FA uptake and transfer are unknown, with the exception of peroxisome proliferator–activated receptor (PPAR) γ, whose activities are not restricted to the heart.[23] We identified 2 novel transcriptional regulators of the gene signature and metabolic substrate transport in heart ECs, that is, *Meox2* and *Tcf15*. They both have been described to play a role in the specification of paraxial mesoderm to somitic dermomyotome, and a defect in heart development has not been reported in *Meox2*- or *Tcf15*-deficient mice.[24–26] Meox2 participates in EC homeostasis,[27,28] whereas *Tcf15* has never been studied in ECs, except that it was cloned from an endothelial library.[29] Here, we demonstrate that, within the adult heart, Meox2 and Tcf15 are exclusively expressed in ECs, and that they are critical regulators of FA transport across cardiac ECs.

Methods

An extended Methods text is available online, which includes Table I in the online-only Data Supplement (antibodies) and Table II in the online-only Data Supplement (quantitative real-time polymerase chain reaction primers).

Animal/Human Biopsies

ECs for expression profiling were sorted from *Tie2-GFP* mice. *Meox2^{Cre/+}* mice (referred to as *Meox2^{+/–}*; C57Bl/6) were obtained from the Jackson Laboratories and *Tcf15^{+/–}* mice (129S7/SvEvBrd*C57Bl/6) were provided by E. N. Olson/A. Rawls (Dallas, TX/Tempe, AZ).[24] Human biopsies obtained under informed consent were handled according to the Helsinki Declaration. Procedures were approved by the Ethics Committees of KULeuven for Animal Use, or University Hospitals Leuven.

Cell Isolation/Culture

ECs were sorted by fluorescence-activated cell sorting based on Tie2-GFP fluorescence or antibodies, or selected with antibody-conjugated magnetic beads. Cells were collected in RNA extraction buffer or collection buffer for protein extraction or FA-uptake experiments. Cardiomyocytes were isolated by using a Langendorff perfusion setup. For in vitro studies, human heart ECs and human umbilical vein ECs were grown in EBM2 medium supplemented with EGM2-MV bullet-kit on gelatin-coated plates, and cardiomyocytes were plated on laminin-coated dishes in protein-supplemented M199 medium.

Microarray

Mouse genomewide microarrays on ECs were performed by the VIB Nucleomics Core, as described in the online-only Data Supplement. Functional annotation analysis was done on the validated heart EC gene list with the use of DAVID software (http://david.abcc.ncifcrf.gov/).

RNA/Protein/cDNA Preparation, Quantitative Real-Time Polymerase Chain Reaction, Western Blot, Enzyme-Linked Immunosorbent Assay, and Enzymatic Activity Assays

Total RNA was extracted with RLT or TRIzol, retrotranscribed using SuperscriptIII Reverse Transcriptase, and quantitative real-time polymerase chain reaction was performed with SYBR-Green master mix. For Western blot, total proteins were extracted with radioimmunoprecipitation assay buffer containing protease inhibitors. Human apolipoprotein B and mouse lipoprotein lipase (Lpl) protein were measured by enzyme-linked immunosorbent assay, and Lpl activity was measured with a colorimetric kit.

Lentiviral Overexpression/*siRNA* Knockdown

The construct for overexpressing human *MEOX2* was purchased (Genecopoeia). Open reading frames for human *WT1*, *EBF3*, and murine *Tcf15* were cloned from cDNA-containing plasmids (Thermo Scientific), and *PPARG1* (further referred to as *PPARG*) was cloned from human heart EC cDNA. Lentiviruses were produced in HEK293 cells. Lentiviral transduction, lysate harvesting, and *siRNA* knockdown of *CD36* or *LPL* were performed as described in the online-only Data Supplement.

Proximity Ligation Assay/GST Pull-Down Assays

Proximity ligation assay was performed as previously described[30] in human umbilical vein ECs overexpressing MEOX2 and FLAG-tagged Tcf15 or PROX1. Glutathione *S*-transferase (GST) pull-down assays were performed in HEK293 cells transfected with plasmids encoding GST-tagged Tcf15, FLAG-tagged MEOX2, or both.

In Vitro/Ex Vivo FA Uptake/Transport

FA uptake was analyzed as described in the online-only Data Supplement in cultured human heart ECs 72 hours posttransduction or after *siRNA* treatment, in freshly isolated magnetically selected murine heart ECs or in adult murine cardiomyocytes, 4 hours after plating. FA transport in EC mono- or coculture with cardiomyocytes was analyzed as described in the online-only Data Supplement.

Histology

Immunofluorescence and Sirius red staining were performed on 3- to 6-μm paraffin sections. Oil Red O staining was performed on 10-μm cryosections as described in the online-only Data Supplement.

Echocardiography

Mice (n=8–9; analyzed at 3–4 and 11 months of age) were sedated with 1.5% isoflurane and standard views were obtained in 2 dimensions by transthoracic echocardiography by using an MS400 transducer on a Vevo2100 scanner. Image analysis was performed by a blinded investigator using VisualSonics software.

FA/Glucose Uptake

For FA uptake assessment in vivo, mice were injected intravenously with ^{14}C-oleic acid (OA) or [^{3}H]OA, and, after 30 minutes, radioactivity in different organs/plasma was measured on an LKB-Wallac-Rackbeta-1214 Counter or hearts were harvested and processed for semithin sectioning and autoradiography. Glucose uptake was determined by positron emission tomography imaging during 1 hour after intravenous injection of 2-deoxy-2-[^{18}F]fluoro-ᴅ-glucose.

Statistics

Data are expressed as mean±standard error of the mean from pooled data of 3 to 12 independent experiments. Data normality was supported by the Shapiro-Wilk test (larger samples) or evidence from literature
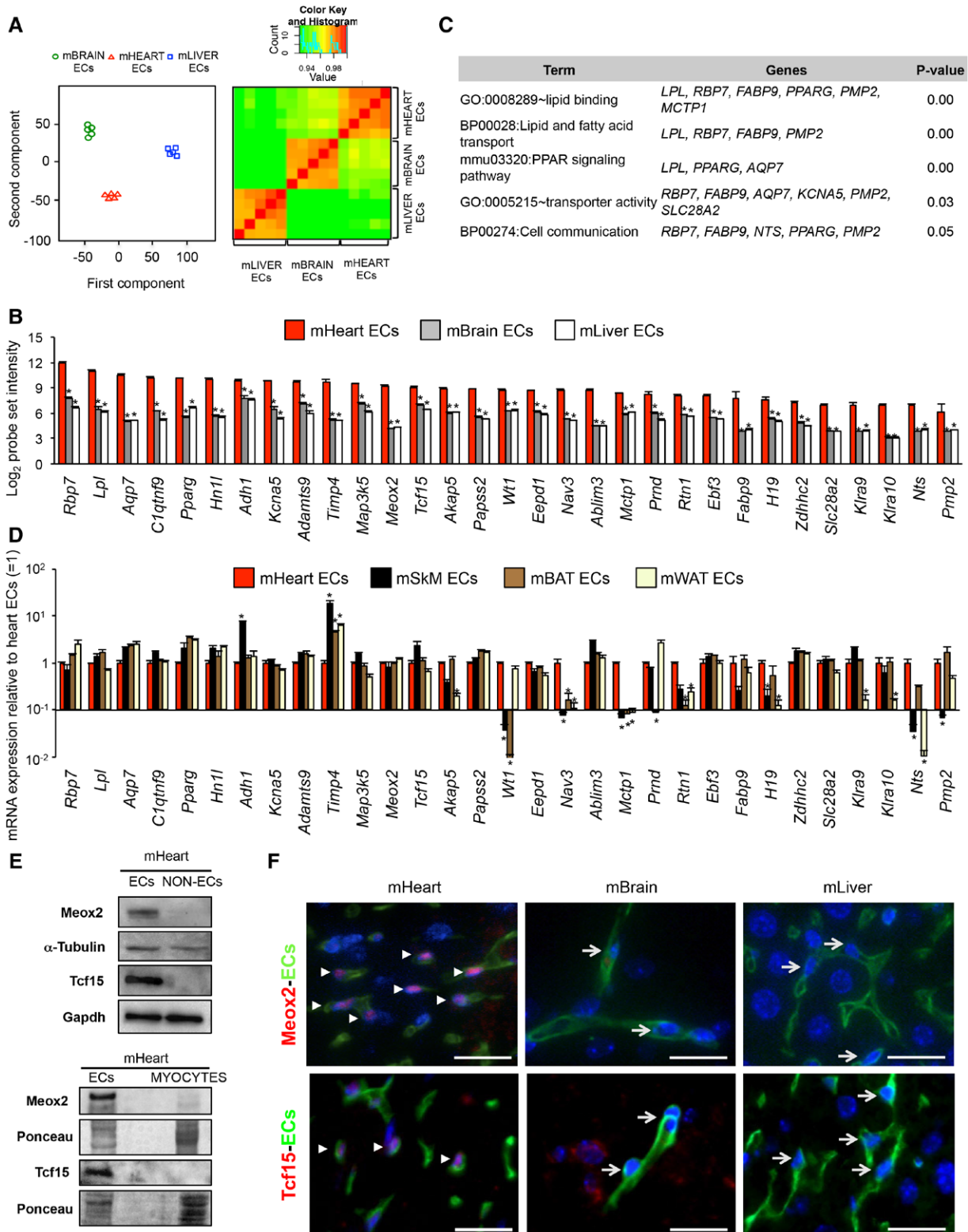
Figure 1. The heart EC fingerprint is enriched in lipid transport–related genes. **A**, Principal component diagram and heat map from a microarray on freshly isolated ECs from murine (m) heart, brain, and liver (n=5). **B**, Log$_2$ probe set intensity of validated genes from the heart EC fingerprint in murine heart, liver, and brain ECs (n=5;*P<0.05 vs heart ECs). **C**, Functional annotation of significantly enriched gene categories from the heart EC fingerprint. **D**, mRNA expression (qRT-PCR) of heart EC fingerprint genes in SkM, BAT, or WAT relative to heart ECs (n=3–4;*P<0.05 vs heart ECs and a minimum 4-fold difference). **E**, Western blots of Meox2, Tcf15, housekeeping protein expression (α-Tubulin/Gapdh), or loading control (Ponceau) in sorted ECs and non-ECs from the heart or freshly isolated cardiomyocytes. **F**, Immunofluorescence stainings for Meox2 or Tcf15 (red; white arrowheads) in murine heart, liver, and brain tissue (ECs stained by lectin in green; arrows indicate EC nuclei). Scale bars, 20 μm. Quantitative data represent mean±standard error of the mean. BAT indicates brown adipose tissue; EC, endothelial cell; qRT-PCR, quantitative real-time polymerase chain reaction; SkM, skeletal muscle; and WAT, white adipose tissue.
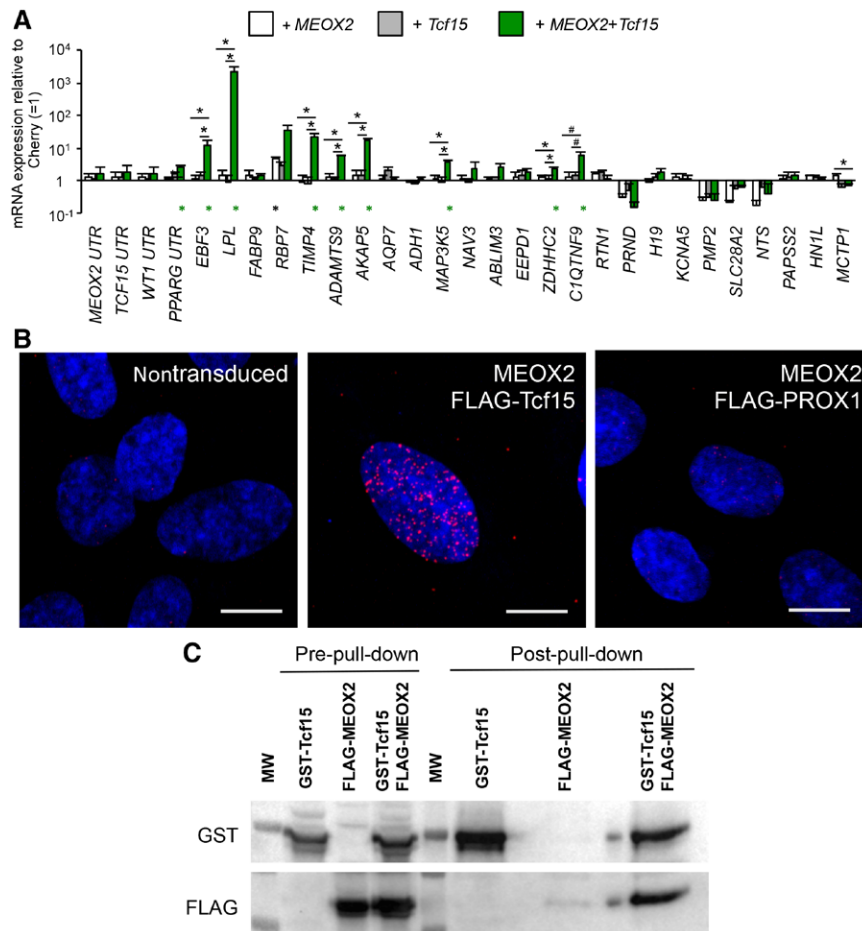
Figure 2. Meox2/Tcf15 heterodimers regulate the heart EC fingerprint in vitro. **A**, Diagram representing mRNA expression (qRT-PCR) for the heart EC fingerprint in cultured human heart ECs overexpressing *MEOX2*, *Tcf15*, or *MEOX2+Tcf15* vs 'Cherry' control. (n=3–9; *$P<0.027$, #$P<0.05$ vs Cherry shown under the bars; or versus another condition as indicated above the bars. $P<0.027$ was considered significant [α']). **B**, Representative pictures of a Proximity Ligation Assay (PLA) on HUVECs (nuclei stained with TO-PRO in blue) showing no red PLA signal in nontransduced cells (Left) or cells overexpressing MEOX2 and PROX1 (Right), whereas the red nuclear dots (Middle) correspond to MEOX2/Tcf15 heterodimers. Scale bars, 10 μm. **C**, Western blot for GST (Top) and FLAG (Bottom) of protein lysates from a GST pull-down assay in HEK293 cells overexpressing GST-Tcf15, FLAG-MEOX2, or both, showing prepull-down total protein lysate samples (Left) and post-GST pull-down samples (Right). Quantitative data represent mean±standard error of the mean. EC indicates endothelial cell; GST, glutathione *S*-transferase; HUVEC, human umbilical vein endothelial cell; MW, molecular weight; and qRT-PCR, quantitative real-time polymerase chain reaction.

reporting on analogous data sets (smaller samples). For single comparisons, the homogeneity of group variances was determined with the Levene test and *P* values were calculated with the Welch *t* test or the 2-tailed (un)paired Student's *t* test where appropriate. For time courses of a single variable comparison, repeated-measures analysis of variance was applied, followed by Student's *t* test for each time point. $P<0.05$ was considered significant. For multiple comparisons, *P* values were calculated with a priori nonorthogonal contrast analysis (with the type of comparisons predetermined based on biological relevance and indicated in the figure legends), after 1-way analysis of variance and the Levene test. The significance level α (0.05) was corrected for multiple comparisons with the Keppel-modified Bonferroni test and the resulting α′ is indicated in the figure legends where appropriate.

Results

Gene Signature of Heart Capillary ECs

To obtain a heart microvascular EC signature, we performed a microarray comparison of pure populations of GFP+ ECs freshly isolated from the hearts, livers, and brains of adult *Tie2-GFP* mice (Figure IA through IC and Note I in the online-only Data Supplement) revealing a high degree of heterogeneity between vascular beds (Figure 1A). After filtration (by defining as a threshold a minimum Log₂ probe set intensity of 6 and a minimum 4-fold difference in comparison with brain and liver ECs [$P<0.05$]) and quantitative real-time polymerase chain reaction validation of the gene list (only genes significantly enriched in the EC fraction in comparison with non-ECs and/or cardiomyocytes were retained [$P<0.05$], data

not shown), we obtained a set of 31 genes enriched in heart capillary ECs (Figure 1B). Functional annotation revealed that the main functions represented were lipid binding and lipid/FA transport (Figure 1C). To consolidate this signature, we measured its expression in ECs freshly isolated from additional tissues, ie, pancreas, lung, and kidney. We found that most genes (81% in comparison with at least 2 tissues, 48% in comparison with all 3 tissues) were at least 4-fold enriched in heart ECs (Figure ID in the online-only Data Supplement). On the other hand, ECs isolated from tissues with continuous endothelium that, like the heart, are highly active in FA uptake for energy production or storage (ie, skeletal muscle or SkM, brown and white adipose tissue or BAT and WAT, respectively) showed for most genes an expression level similar to that in heart ECs (Figure 1D). Cross-species validation in human ECs confirmed a partially retained enrichment of the signature in human heart in comparison with brain and liver ECs (Figure IIA in the online-only Data Supplement). Finally, as for other EC types,[2,31,32] human heart ECs lost their specific gene expression profile upon culturing (Figure IIB in the online-only Data Supplement).

Transcriptional Regulation of Heart EC Identity In Vitro

In addition to FA transport-related genes, the signature contained 5 TF-encoding genes, ie, *Meox2*, *Tcf15*, *early B-cell factor 3* (*Ebf3*), *Pparg* and *Wilms tumor 1* (*Wt1*; Figure 1B).
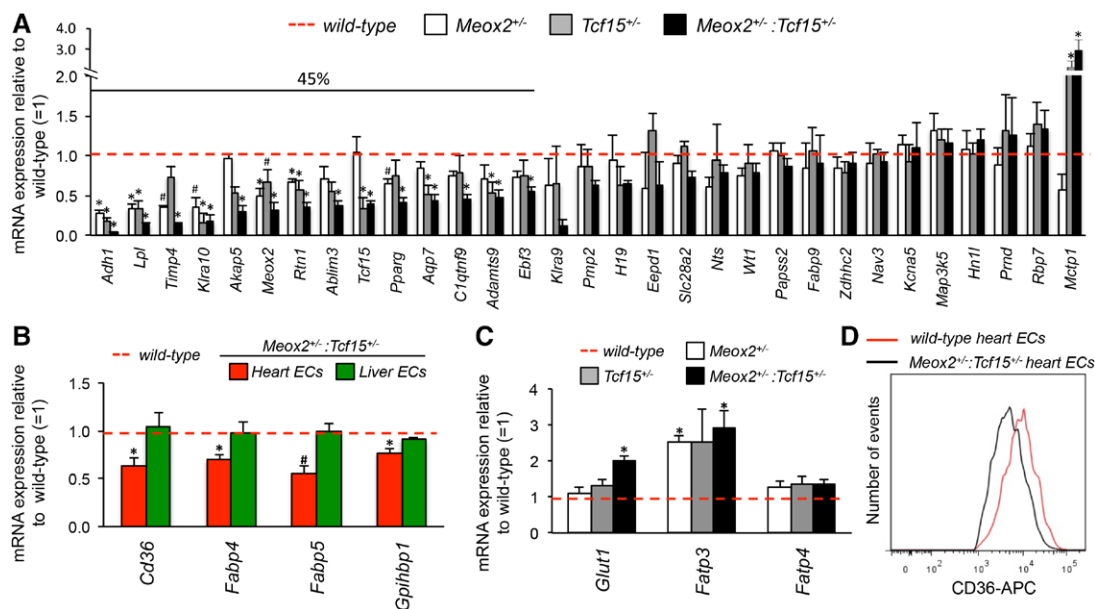
Figure 3. Meox2/Tcf15 regulate heart EC identity in vivo. **A**, mRNA expression (qRT-PCR) of heart EC fingerprint genes in heart ECs from *Meox2+/−*, *Tcf15+/−*, or *Meox2+/−:Tcf15+/−* mice relative to wild-type littermates (n=3–8;*P<0.05, #P<0.1 vs wild-type). **B** and **C**, mRNA expression (qRT-PCR) in heart (**B** and **C**) or liver ECs (**B**) from *Meox2+/−:Tcf15+/−* mice relative to wild-type littermates (n=5–8 for **B**; n=3 for **C**; *P<0.05, #P<0.1 vs wild-type). **D**, Histogram overlay representative for n=3 showing reduced CD36 protein in heart ECs from *Meox2+/−:Tcf15+/−* mice vs wild-type littermates. Quantitative data represent mean±standard error of the mean. APC indicates allophycocyanin; EC, endothelial cell; and qRT-PCR, quantitative real-time polymerase chain reaction.

We confirmed by tissue immunostaining and Western blot on sorted cells that Meox2 and Tcf15 were exclusively expressed in the EC compartment of the murine heart and undetectable in liver or brain ECs (Figure 1E and 1F and Figure III in the online-only Data Supplement). We next tested whether these TFs would intrinsically regulate the heart EC signature by assessing whether their overexpression would restore the fingerprint in human heart ECs in which it was erased by culturing. Overexpressing *MEOX2* or *Tcf15* alone did not affect signature gene expression; however, when overexpressed in combination, 31% of the genes were significantly upregulated (Figure 2A). Proximity ligation assay and GST pull-down revealed that this cooperative effect involved heterodimeric complex formation (Figure 2B and 2C). *MEOX2* or *Tcf15* did neither affect each other's expression nor that of *WT1*, but had a small yet significant inductive effect on *PPARG*. *EBF3* was strongly induced by *MEOX2+Tcf15*. Yet, its overexpression induced a limited number of signature genes and thus did not recapitulate the effect of *MEOX2+Tcf15*. Furthermore, combining *EBF3* overexpression with *MEOX2+Tcf15* did not have an additive effect (Figure IVA in the online-only Data Supplement). We also studied the inductive effect of *PPARG* and the most abundant *WT1* isoform (Note II in the online-only Data Supplement). *PPARG* and *WT1* overexpression partially induced the heart EC fingerprint (Figure IVB and IVC in the online-only Data Supplement). Moreover, *PPARG* exerted a synergistic effect with *MEOX2+Tcf15,* whereas *WT1* did not have an additive effect on *MEOX2+Tcf15+PPARG* overexpression. Upregulation for a random gene subset was confirmed at protein level (Figure IVD in the online-only Data Supplement). *MEOX2+Tcf15* overexpression induced the heart EC signature in human umbilical vein ECs to a similar extent as in cultured heart ECs (Figure IVE in the online-only Data Supplement).

Meox2/Tcf15 Determine Heart EC Identity In Vivo

To address whether Meox2 and Tcf15 cooperated to affect the heart EC expression profile in vivo, mice lacking 1 allele of each factor were generated. Mice homozygously deficient for *Tcf15*[24] or *Meox2* (online-only Data Supplement Note III) die perinatally, while combined heterozygously deficient mice are viable. ECs were isolated from hearts and, as a control, from livers of adult *Meox2+/−:Tcf15+/−* mice and their single-heterozygous or wild-type littermates and their gene expression profile were analyzed by quantitative real-time polymerase chain reaction. Although haplodeficiency for *Meox2* or *Tcf15* alone only slightly affected the heart EC signature, we observed a significant downregulation of 45% of the signature genes in *Meox2+/−:Tcf15+/−* hearts, supporting the cooperative interaction of both TFs also in vivo (Figure 3A). Complementary to our in vitro findings, *Pparg* and *Ebf3* were significantly downregulated, whereas *Wt1* was not affected, confirming the TF hierarchy we unraveled in vitro (Figure 2A). General EC markers were not affected in heart ECs, and liver sinusoidal EC-specific genes were not altered in liver ECs (Figure VA and VB in the online-only Data Supplement), suggesting that Meox2/Tcf15 specialize ECs in the heart, while neither affecting EC identity per se, nor EC specialization in unrelated tissues.

Meox2+Tcf15 Haplodeficiency Alters Energy Substrate Transporter Gene Expression in Heart ECs In Vivo

Because FA transport emerged as a principal function associated with the heart EC signature, we further investigated whether *Meox2+Tcf15* haplodeficiency altered endothelial expression of additional genes encoding FA or glucose transport–related

molecules, previously described in heart ECs but not included in our signature, either because of not being enriched in heart ECs in comparison with both liver and brain ECs, or because of being <4-fold enriched (Figure VC in the online-only Data Supplement). FA translocase *CD36*,[15,18,19] cytoplasmic FA binding protein *Fabp4*[33] and *Gpihbp1*, encoding the transporter and anchoring protein for Lpl on the luminal EC surface,[34] were significantly downregulated in *Meox2+/–:Tcf15+/–* heart, but not in liver ECs, whereas *Fatp3*, a FA transporter regulated by VEGF-B interaction with heart ECs,[21] and the glucose transporter *Glut1* were upregulated in *Meox2+/–:Tcf15+/–* heart ECs (Figure 3B and 3C). Expression of *Fatp4*, another FA transporter gene induced by VEGF-B,[21] was not affected by *Meox2+Tcf15* haplodeficiency (Figure 3C). Reduced *CD36* expression in *Meox2+/–:Tcf15+/–* heart ECs was confirmed at the protein level (Figure 3D). Together, these observations further suggest a functional role for Meox2+Tcf15 in FA (and glucose) transfer in and through heart ECs.

Meox2/Tcf15 Drive Free FA Uptake in and Transport Across ECs

To demonstrate that Meox2/Tcf15 are functionally important for FA trafficking, we next determined whether free FA (FFA)

uptake in cultured human heart ECs could be enhanced by their overexpression. As measured by fluorescence-activated cell sorting, uptake of bovine serum albumin-bound fluorescently labeled dodecanoic acid was increased by 150% upon *MEOX2+Tcf15* overexpression (Figure 4A). Additionally, freshly isolated heart ECs from *Meox2+/–:Tcf15+/–* mice showed a 19% decrease in FFA uptake in comparison with those of wild-type littermates (Figure 4B). Because *CD36* expression in the heart ECs of *Meox2+/–:Tcf15+/–* mice was significantly lowered (Figure 3B and 3D), whereas it was upregulated upon combined *MEOX2+Tcf15* overexpression in cultured heart ECs and human umbilical vein ECs (unlike other transporters; Figure VIA and VIB in the online-only Data Supplement and data not shown), and because *CD36* is the FA transporter expressed at the highest level in heart ECs (>200-fold higher than any other FA transporter; Figure VIC in the online-only Data Supplement), we investigated whether *CD36* was involved in Meox2/Tcf15-driven FFA uptake. *CD36* knockdown reduced FFA uptake by 12% in heart ECs overexpressing *MEOX2+Tcf15*, meaning that CD36 accounted for ≈20% of the uptake caused by combined *MEOX2+Tcf15* overexpression (Figure 4C). Using an in vitro transwell assay, we deliver proof that Meox2/Tcf15 also affected FFA transport
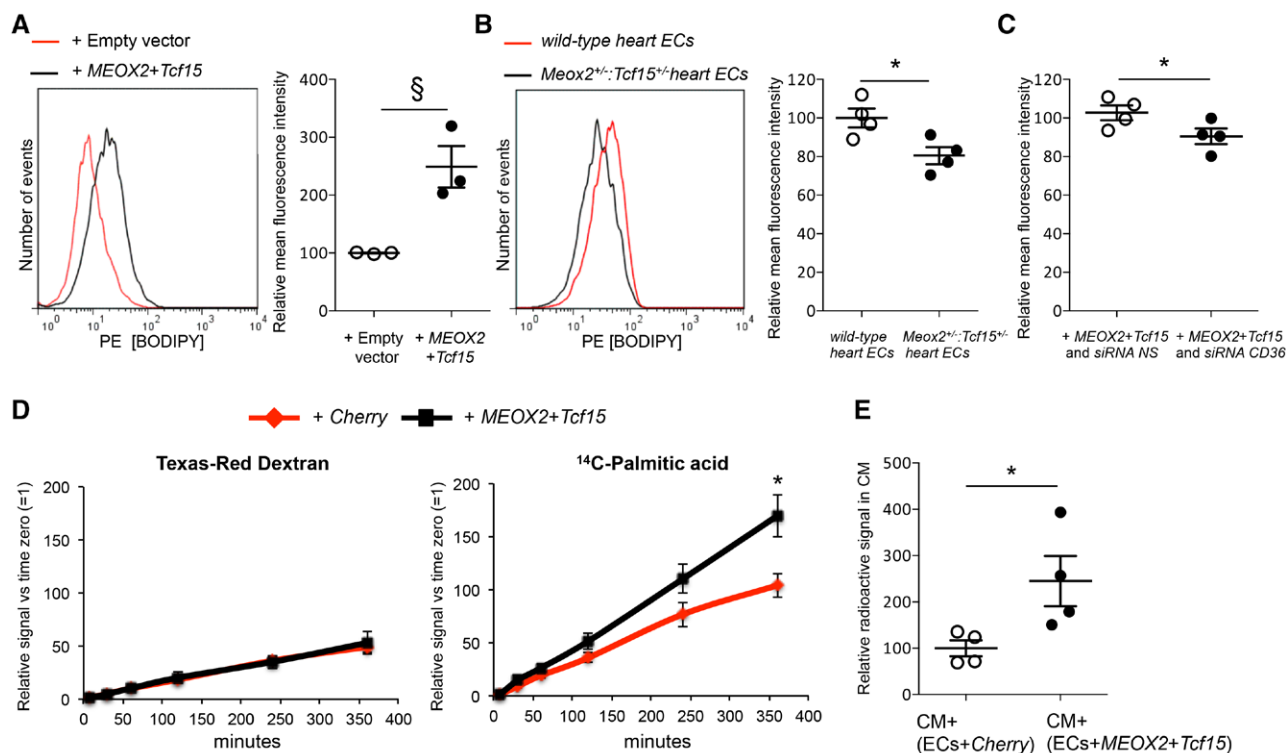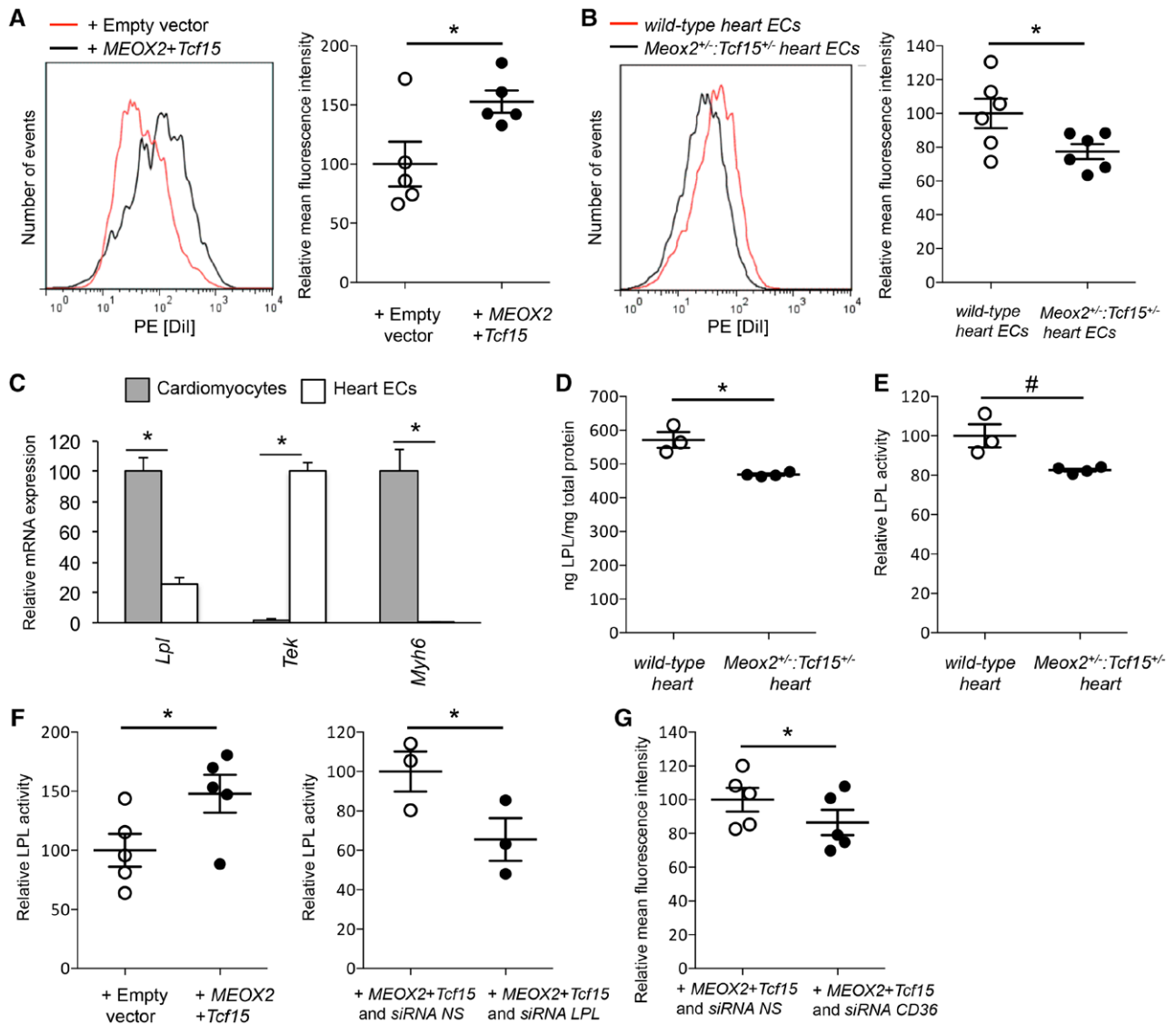

Figure 4. Meox2/Tcf15 regulate free FA uptake and transport in ECs. **A**, Representative histogram overlay showing BODIPY-dodecanoic acid (DA) uptake by cultured human heart ECs transduced with empty or *MEOX2+Tcf15* lentiviral vectors and corresponding quantification of mean fluorescence intensity (MFI; n=3; §*P*=0.053 vs empty vector). **B**, Representative histogram overlay showing BODIPY-DA-uptake by freshly isolated heart ECs from wild-type and *Meox2+/–:Tcf15+/–* mice and corresponding MFI quantification (n=4; **P*<0.05 vs wild-type). **C**, Quantification of BODIPY-DA-uptake in human heart ECs overexpressing *MEOX2+Tcf15* transfected with a nonsilencing (NS) or a *siRNA-CD36* construct (n=4; **P*<0.05 vs NS). **D**, Time course of Texas-Red Dextran and ^{14}C-palmitic acid accumulation in the lower well of a transwell chamber, transported through a monolayer of HUVECs transduced with Cherry or *MEOX2+Tcf15* lentiviruses. Data are expressed relative to the signal at time zero. (n=3; **P*<0.05 vs Cherry). **E**, Relative radioactivity in cardiomyocytes (CM) cocultured with HUVECs (ECs) transduced with Cherry or *MEOX2+Tcf15* lentiviruses and preloaded with ^{14}C-OA. Data are expressed as relative signal vs CM cocultured with ECs+Cherry. (n=4; **P*<0.05 vs CM+[ECs+Cherry]). Quantitative data represent mean±standard error of the mean. EC indicates endothelial cell; FA, fatty acid; HUVEC, human umbilical vein endothelial cell; OA, oleic acid; and PE, phycoerythrin.

across an endothelial monolayer (Figure 4D). Finally, with a coculture system we showed that Meox2/Tcf15 regulate the capacity of ECs to take up and transfer FFAs to cardiomyocytes (Figure 4E).

Meox2/Tcf15 Regulate VLDL-Derived FA Uptake in Heart ECs

FAs reach the heart EC barrier not only bound to albumin (FFAs) but also esterified in the triacylglycerol core of circulating lipoproteins (eg, chylomicrons or very-low-density lipoproteins [VLDL]). We determined whether Meox2/Tcf15 could regulate VLDL-derived FA uptake by measuring the uptake of 1,1'-Dioctadecyl-3,3,3',3'-Tetramethylindocarbocyanine Perchlorate (DiI) signal incorporated in the lipidic parts of DiI-labeled VLDL. *MEOX2+Tcf15* overexpression in cultured heart ECs induced an increase of DiI uptake by 53% (Figure 5A), and, accordingly, in heart ECs freshly isolated from *Meox2+/−:Tcf15+/−* mice, DiI uptake was decreased by 22% in comparison with wild-type mice (Figure 5B). It is known that in vivo, triglyceride-derived FAs from VLDL can be taken up by tissues either as a component of nascent or remnant lipoprotein particles or as FFAs following Lpl-mediated triglyceride lipolysis at the

Figure 5. Meox2/Tcf15 regulate VLDL-derived FA uptake in heart ECs. **A** and **B**, Representative histogram overlays showing DiI-VLDL uptake in cultured human heart ECs transduced with empty or *MEOX2+Tcf15* lentiviral vectors and corresponding MFI quantification (n=5; *P<0.05 vs empty vector; **A**), and in freshly isolated heart ECs from wild-type and *Meox2+/−:Tcf15+/−* mice and corresponding MFI quantification (n=6; *P<0.05 vs wild-type; **B**). **C**, Diagram representing qRT-PCR on freshly isolated cardiomyocytes and heart ECs (n=3; *P<0.05 vs cardiomyocytes). **D**, Quantification of LPL protein content in wild-type and *Meox2+/−:Tcf15+/−* hearts. (n=3–4; *P<0.05 vs wild-type). **E**, Relative LPL activity in wild-type and *Meox2+/−:Tcf15+/−*hearts (n=3–4; #P<0.1 vs wild-type). **F**, Bar graphs representing relative LPL activity in cultured heart ECs transduced with empty vector or *MEOX2+Tcf15* (Left) or in *MEOX2+Tcf15* overexpressing heart ECs transfected with a nonsilencing (NS) or a *siRNA-LPL* construct (Right; n=3–5; *P<0.05 vs empty vector or NS). **G**, Quantification of DiI-VLDL uptake in human heart ECs overexpressing *MEOX2+Tcf15* transfected with either a nonsilencing (NS) or an *siRNA-CD36* construct (n=5; *P<0.05 vs NS). Quantitative data represent mean±standard error of the mean. EC indicates endothelial cell; FA, fatty acid; LPL, lipoprotein lipase; MFI, mean fluorescence intensity; PE, phycoerythrin; qRT-PRC, quantitative real-time polymerase chain reaction; and VLDL, very-low-density lipoproteins.

luminal EC surface.[34–36] In our in vitro system, VLDL particle uptake occurred and *MEOX2+Tcf15* overexpression tended to increase this, as shown by the uptake of Apolipoprotein B protein, but this increase was not significant (Figure VIIA in the online-only Data Supplement). On the other hand, we found *Lpl* mRNA expression in pure heart ECs (Figure 1B), the levels of which were 25% of those in pure cardiomyocytes (Figure 5C). Because, in comparison with wild-type, *Meox2+/-:Tcf15+/-* hearts show a downregulation of *Lpl* mRNA by 90% in their EC but not cardiomyocyte fraction (Figure 3A and Figure VIIIA in the online-only Data Supplement) and had an ≈18% decrease in Lpl protein and activity (Figure 5D and 5E), we estimated that EC-derived Lpl activity is ≈20% of that in the total heart. Furthermore, *MEOX2+Tcf15* overexpression in cultured heart ECs increased lipoprotein lipase (LPL) activity by 48%, and this increase was completely neutralized upon *LPL* knockdown (Figure 5F). Together, these results support the production of active Lpl by heart ECs and its regulation by Meox2/Tcf15. To demonstrate that this EC-produced LPL-hydrolyzing activity was involved in *MEOX2+Tcf15*-driven VLDL-derived FFA uptake, we knocked down *CD36*, an important downstream mediator of LPL-generated FFAs that is not involved in VLDL particle uptake[35] (Figure VIIB in the online-only Data Supplement). *CD36* knockdown in *MEOX2+Tcf15*–overexpressing heart ECs

decreased the DiI signal by 13% (Figure 5G). Together, these data demonstrate an EC-autonomous role for Meox2/Tcf15-regulated Lpl in VLDL-derived FFA uptake.

Meox2/Tcf15 Regulates Cardiac Energy Substrate Uptake In Vivo

To evaluate whether *Meox2+Tcf15* haplodeficiency altered FA uptake in the heart in vivo, we administered ^{14}C-OA via tail vein injection to 12- to 16-week-old *Meox2+/-:Tcf15+/-* and wild-type males, and measured the radioactive signal in different organs after 30 minutes. FA uptake was significantly decreased in the heart (by 35%), and was also decreased (by 50%) in oxidative SkM (soleus) in *Meox2+/-:Tcf15+/-* mice – as expected by the fact that Meox2 and Tcf15 are also expressed in the SkM endothelium, which also expresses the other genes of the heart EC signature at high levels (Figure 6A). Unexpectedly, however, FA uptake was significantly increased (by ≈100%) in BAT of *Meox2+/-:Tcf15+/-* mice, although BAT ECs had similar levels of expression of the genes of the heart EC fingerprint and FA transporters than heart ECs, and showed downregulation of, eg, *CD36* and *Lpl* in *Meox2+/-:Tcf15+/-* mice (Figure 1D and Figure IXA and IXB in the online-only Data Supplement). Other organs had a similar uptake in the 2 genotypes. Although we detected a 22% increase in radioactive signal in plasma of *Meox2+/-:Tcf15+/-* mic, which
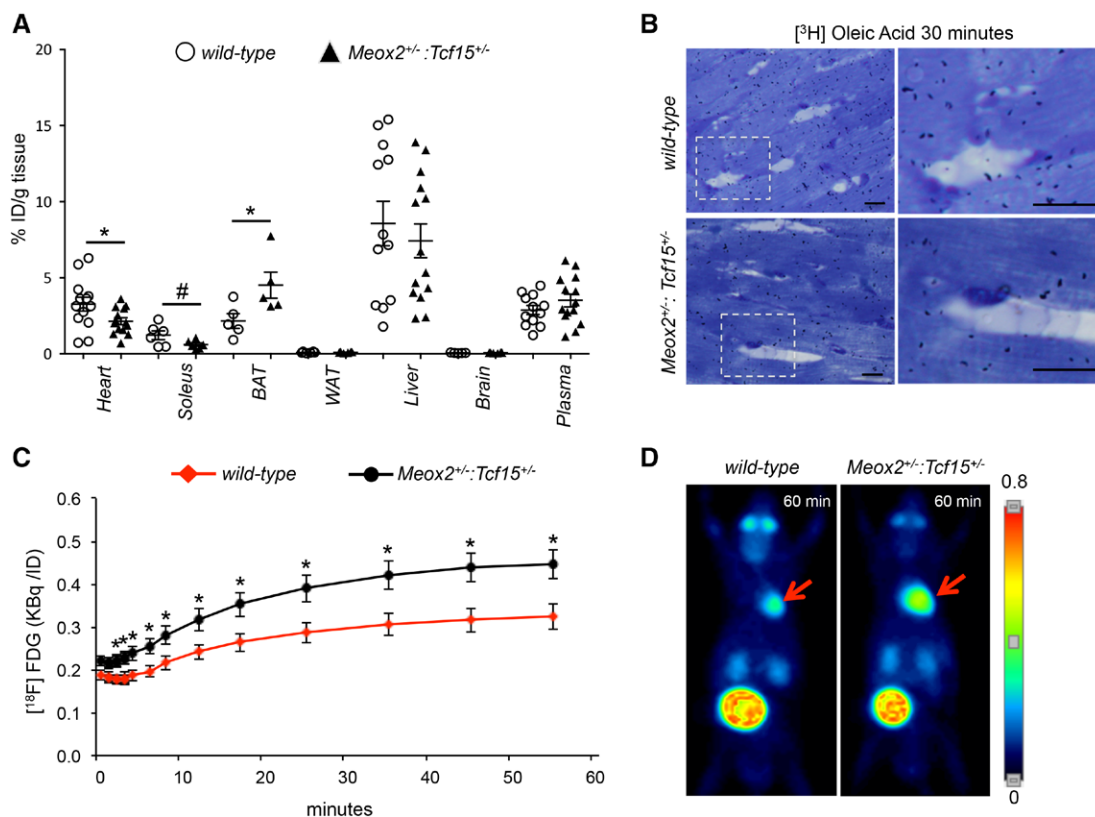
Figure 6. Meox2/Tcf15 regulate cardiac energy substrate uptake in vivo. **A,** Diagram showing the amount of radioactivity in hearts from *Meox2+/-:Tcf15+/-* or wild-type littermates, expressed as percentage of injected ^{14}C-oleic acid (OA) dose (ID) per gram (n=5–14; *P<0.05, #P<0.1 vs wild-type). **B,** Representative autoradiography pictures on semithin sections (with corresponding insets on the right) of wild-type and *Meox2+/-:Tcf15+/-* hearts 30 minutes after [3H]OA injection. Scale bars, 10 μm. **C** and **D,** Time-lapse quantification (**C**) of [18F]FDG uptake into *Meox2+/-:Tcf15+/-* or wild-type hearts (n=11–12; *P<0.05 vs wild-type) and representative small-animal PET images (**D**) of wild-type and *Meox2+/-:Tcf15+/-* hearts (arrows) 60 minutes after injection. Quantitative data represent mean±standard error of the mean. [18F]FDG indicates 2-deoxy-2-[18F]fluoro-D-glucose; and PET, positron emission tomography.

could suggest a slower clearance of plasma FAs by peripheral tissues, this increase was not statistically significant (*P*=0.24). Autoradiography on semithin sections of *Meox2+/−:Tcf15+/−* and wild-type littermate hearts confirmed that there was much less FA signal in *Meox2+/−:Tcf15+/−* hearts 30 minutes after [³H]OA injection and furthermore shows that the signal almost exclusively originated from cardiomyocytes, with no accumulation of FAs in the extracellular space, suggesting that FA uptake by cardiomyocytes was not compromised (Figure 6B). Accordingly, expression of none of the lipid or glucose transport–related genes tested was affected in *Meox2+/−:Tcf15+/−* cardiomyocytes and they did not have an impaired FA uptake in vitro (Figure VIIIA and VIIIB in the online-only Data Supplement). Together, these data suggest that, in *Meox2+/−:Tcf15+/−* mice, FA delivery from the plasma to cardiomyocytes is impaired because of a reduced passage through the endothelium. To investigate whether reduced FA delivery was compensated by increased glucose uptake, we measured 2-deoxy-2-[¹⁸F]fluoro-D-glucose uptake in the heart, and detected a 38% increase in *Meox2+/−:Tcf15+/−* in comparison with wild-type mice at ≈60 minutes postinjection (Figure 6C and 6D).
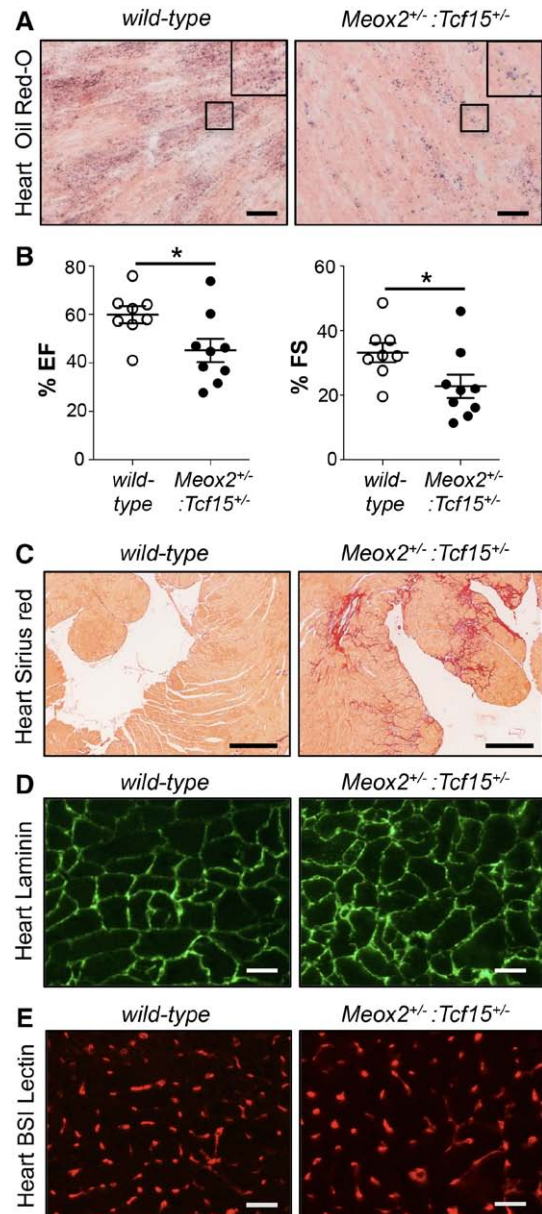
Aged *Meox2+/−:Tcf15+/−* Mice Develop Cardiac Dysfunction

Because an altered energy substrate use could be associated with cardiac dysfunction in animal models upon aging,[17,36] we performed histological and functional analysis on young and aged *Meox2+/−:Tcf15+/−* and wild-type males. In accordance with the in vivo ¹⁴C-OA uptake assay, Oil Red O staining revealed a decrease in lipid accumulation in heart muscle of *Meox2+/−:Tcf15+/−* in comparison with wild-type hearts both in young (Figure XA in the online-only Data Supplement) and aged mice (Figure 7A). However, although young mice displayed normal cardiac function and histology (Figure XB and XC and Table III in the online-only Data Supplement), aged (44 weeks old) *Meox2+/−:Tcf15+/−* mice displayed heart systolic dysfunction, as evidenced by a reduced ejection fraction and fractional shortening, sporadically accompanied by fibrosis and associated with a slight decrease in capillary density, but no significant differences in cardiomyocyte size (Figure 7 and Tables III and IV in the online-only Data Supplement).

Discussion

To improve the understanding of EC heterogeneity between capillaries of different organs, we here report a fingerprint of genes enriched in heart microvascular ECs, which is largely shared with ECs of SkM, BAT, and WAT, all tissues highly active in FA uptake for energy production or storage. We show that Meox2 and Tcf15, by interacting as a heterodimeric complex, EC-autonomously determine the expression of these fingerprint genes both in vitro and in vivo, while individually they had only a minor effect.

Our in vitro and ex vivo mechanistic studies showed that Meox2/Tcf15 intrinsically regulate uptake by cardiac ECs of FFAs originating from both bovine serum albumin conjugates and EC-derived Lpl hydrolysis of triglycerides contained in VLDL particles (Figure 8). Although the finding of EC-derived Lpl challenges the currently prevailing view that cardiomyocytes are the sole cardiac source of Lpl,[34] we estimated that

Figure 7. Aged *Meox2+/−:Tcf15+/−* mice develop cardiac dysfunction. **A**, Oil Red O (ORO)–stained cross-sections of wild-type or *Meox2+/−:Tcf15+/−* hearts. Scale bars, 20 μm. **B**, Echocardiographic analysis of wild-type or *Meox2+/−:Tcf15+/−* mice showing % ejection fraction (%EF) and % fractional shortening (%FS; n=8–9; *P<0.05 vs wild-type). **C**, Sirius red–stained cross-sections of wild-type or *Meox2+/−:Tcf15+/−* hearts. Scale bars, 500 μm. **D** and **E**, Cross-sections of wild-type or *Meox2+/−:Tcf15+/−* hearts stained with laminin (**D**; basement membranes: green) and corresponding cross-sections of wild-type or *Meox2+/−:Tcf15+/−* hearts stained with BSI lectin (**E**; capillaries: red). Scale bars, 20 μm. Quantitative data represent mean±standard error of the mean. BSI indicates *Bandeiraea simplicifolia*.

EC-derived Lpl protein and activity is ≈20% of that in the whole heart, which is well in line with the observation by Bharadwaj et al[35] that there is ≈14% residual Lpl activity in hearts of cardiomyocyte-specific *Lpl*-deficient mice. Meox2/Tcf15 also potentially regulate the expression of *Gpihbp1*,[34] responsible for Lpl transfer from cardiomyocytes and for its positioning at the luminal surface of heart capillary ECs (Figure 8).
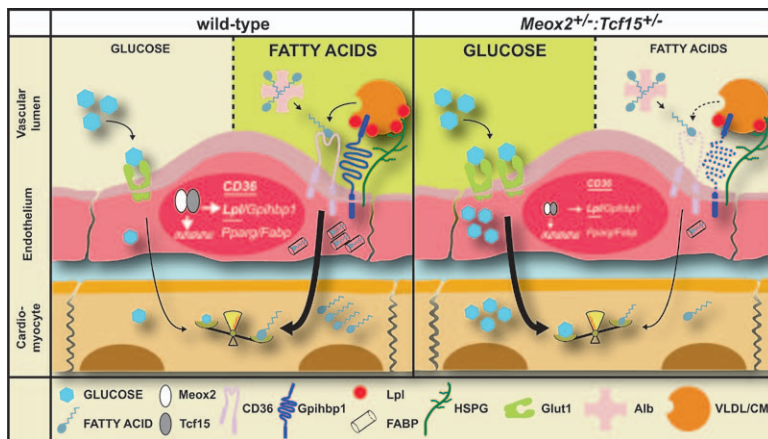
Figure 8. Schematic summary. In wild-type heart endothelial cells (ECs), Meox2/Tcf15 heterodimers regulate the balance between fatty acid (FA) and glucose uptake by orchestrating the expression of multiple transport-related genes, supporting the preferential use of FAs as a source of energy production in cardiomyocytes. Combined *Meox2+Tcf15* heterozygous deficiency results in downregulation of these genes and an increase in *Glut1*, and causes a shift to higher glucose and lower FA delivery to cardiomyocytes. Genes for which we have direct mechanistic proof are underlined. Alb indicates albumin; CM, chylomicron; FABP, fatty acid binding protein; Glut1, glucose transporter 1; HSPG, heparan sulfate proteoglycans; Lpl, lipoprotein lipase; and VLDL, very-low-density lipoprotein.

Using a combination of gain- and loss-of-function experiments, we showed that CD36 is downstream of Meox2/Tcf15-mediated uptake of FFAs originating from both bovine serum albumin conjugates and VLDL particles in heart ECs. The high CD36 expression levels in comparison with other transporter genes in heart ECs further support its important role in cardiac FA uptake. Nevertheless, although, in our DiI-VLDL assay, CD36's contribution to Meox2/Tcf15-driven FFA uptake could have been underestimated by simultaneous detection of particle uptake, the fact that *CD36* knockdown only partially impaired Meox2/Tcf15-driven uptake of BODIPY-labeled FFAs suggests the existence of other Meox2/Tcf15 downstream mediators or the occurrence of compensatory mechanisms upon *CD36* knockdown.

In *Meox2+/−:Tcf15+/−* heart ECs, *Fatp3*, a FA transporter regulated by the paracrine VEGF-B,[21] was increased, but this was not sufficient to fully compensate for the partial loss of CD36 induced by *Meox2+Tcf15* haplodeficiency, because cardiac FA uptake was significantly compromised in the *Meox2+/−:Tcf15+/−* heart. On the other hand, *Fatp4*, another FA transporter regulated by VEGF-B,[21] was not affected by the haploinsufficiency of *Meox2+Tcf15* in heart ECs. Finally, MEOX2+Tcf15 overexpression did not regulate *FATP3* or *FATP4* in vitro (data not shown), whereas VEGF-B is not able to regulate *CD36*.[21] Therefore, we hypothesize that these extrinsic and intrinsic pathways do not overlap in regulating FA uptake in heart ECs. On the other hand, we found that *Pparg*, known to be an intrinsic regulator of EC FA uptake,[23] seemed to be downstream of and synergize with Meox2/Tcf15 to determine the heart EC signature, suggesting a new TF hierarchy in charge of endothelial FA uptake.

Meox2/Tcf15 did not only support FA uptake in, but also transport across ECs, as shown with a transwell assay. In particular, they could regulate the capacity of ECs to take up and transfer FAs to cardiomyocytes, as shown in our in vitro coculture experiments. Meox2/Tcf15-mediated transendothelial transport was likely dependent on CD36-mediated FA uptake and may involve certain fingerprint genes and cytoplasmic FA transporters in charge of FA shuttling from the apical to the basal side of ECs, such as *Fabp4* and *Fabp5*, the loss of which is known to decrease FA uptake in the heart[33] and which were downregulated in heart ECs of *Meox2+/−:Tcf15+/−* mice (Figure 8).

In vivo, *Meox2+Tcf15* haplodeficiency caused decreased FFA uptake in the heart. Surprisingly, despite a similar expression of signature genes and FA transporters in heart and BAT ECs and a common downregulation of *CD36* in ECs of both tissues in *Meox2+/−:Tcf15+/−* mice, FFA uptake was increased in *Meox2+/−:Tcf15+/−* BAT, suggesting that compensatory uptake mechanisms were at play, eg, involving BAT EC-specific genes or environmental factors secreted by brown adipocytes.

Together, our in vitro and ex vivo mechanistic studies in EC mono- or cocultures with cardiomyocytes support the notion that an EC-specific role for Meox2/Tcf15 in FA uptake and transport to cardiomyocytes accounts for the lower cardiac FA uptake measured in adult *Meox2+/−:Tcf15+/−* hearts in vivo. Additional support for such a role is given by the fact that Meox2/Tcf15 expression was undetectable in other cardiac cells and, additionally, expression of genes related to FA transport in freshly isolated *Meox2+/−:Tcf15+/−* cardiomyocytes was unaffected nor was their uptake of FAs – as evidenced in vitro in isolated cardiomyocytes and in vivo by autoradiography. Nevertheless, our in vivo FA uptake studies were performed in ubiquitous and constitutive *Meox2+/−:Tcf15+/−* mice. Hence, we cannot entirely exclude that *Meox2+Tcf15* haplodeficiency during development or in other organs or even in other cell types in the heart could have also contributed to the lower cardiac FA uptake in adult *Meox2+/−:Tcf15+/−* mice. Definitive proof for an isolated cardiac EC-exclusive cause of the diminished cardiac FA uptake would require the generation of cardiac EC-specific, inducible knockout mice.

Interestingly, the reduced FA uptake was compensated by a higher glucose uptake in the heart of *Meox2+/−:Tcf15+/−* mice – possibly due to higher *Glut1* (but not *Glut4*; data not shown) expression in cardiac ECs, suggesting a switch in energy substrate usage in *Meox2+/−:Tcf15+/−* hearts. Even though higher glucose consumption has been proven beneficial for the heart upon cardiac stress,[10,37] chronic adaptation to impaired FA uptake toward higher glucose consumption (like in *Lpl−/−*,[36] *H-Fabp−/−*,[17] or *CD36−/−* [15,18] mice) limits the heart's metabolic flexibility, rendering it more susceptible to events that lead to cardiac metabolic changes, like an insult or aging. Accordingly, *Meox2+Tcf15* haplodeficiency in aged mice resulted in impaired cardiac contractility, sporadically accompanied by fibrosis – likely a late manifestation of cardiac dysfunction. Our current data, however, do not provide

conclusive evidence that the heart phenotype of aged *Meox2*^{+/−}*:Tcf15*^{+/−} mice is related to a defect in adult cardiac EC FA handling, because this would require a conditional genetic approach. Furthermore, other genes regulated by Meox2/Tcf15-encoding proteins whose function is not directly linked to energy substrate delivery could contribute to heart dysfunction/fibrosis, eg, tissue inhibitor of metalloproteinase 4 and metalloproteinase Adamts9, which play a role in matrix remodeling in the heart.[38,39]

In summary, here we provide for the first time a fingerprint of genes enriched in ECs lining capillaries of tissues with high metabolic capacity for FAs, suggesting a common specialization of these vascular beds. We identified Meox2/Tcf15 heterodimers as transcriptional determinants of the heart EC fingerprint and demonstrated that they are critical regulators of FA transport across heart ECs, in part, through the regulation of CD36 and Lpl expression. Combined *Meox2+Tcf15* haplodeficiency resulted in downregulation of these and other FA transport-related genes and an increase of glucose transporter *Glut1* in heart ECs, and a switch of the cardiac energy substrate balance (Figure 8). These findings have broadened our understanding of the genetic identity and physiological role of heart microvascular endothelium and provide a platform for further mechanistic studies for therapeutic exploitation of specific EC targeting aimed at modulating the energy substrate uptake in the heart or promoting heart-specific revascularization.

Disclosures

None.

References

1. Aird WC. Phenotypic heterogeneity of the endothelium: I. Structure, function, and mechanisms. *Circ Res*. 2007;100:158–173. doi: 10.1161/01.RES.0000255691.76142.4a.
2. Géraud C, Schledzewski K, Demory A, Klein D, Kaus M, Peyre F, Sticht C, Evdokimov K, Lu S, Schmieder A, Goerdt S. Liver sinusoidal endothelium: a microenvironment-dependent differentiation program in rat including the novel junctional protein liver endothelial differentiation-associated protein-1. *Hepatology*. 2010;52:313–326. doi: 10.1002/hep.23618.
3. Abbott NJ, Patabendige AA, Dolman DE, Yusof SR, Begley DJ. Structure and function of the blood-brain barrier. *Neurobiol Dis*. 2010;37:13–25. doi: 10.1016/j.nbd.2009.07.030.
4. Brutsaert DL, Fransen P, Andries LJ, De Keulenaer GW, Sys SU. Cardiac endothelium and myocardial function. *Cardiovasc Res*. 1998;38:281–290.
5. Kuruvilla L, Kartha CC. Molecular mechanisms in endothelial regulation of cardiac function. *Mol Cell Biochem*. 2003;253:113–123.
6. Neubauer S. The failing heart–an engine out of fuel. *N Engl J Med*. 2007;356:1140–1151. doi: 10.1056/NEJMra063052.
7. Stanley WC, Recchia FA, Lopaschuk GD. Myocardial substrate metabolism in the normal and failing heart. *Physiol Rev*. 2005;85:1093–1129. doi: 10.1152/physrev.00006.2004.
8. Krishnan J, Suter M, Windak R, Krebs T, Felley A, Montessuit C, Tokarska-Schlattner M, Aasum E, Bogdanova A, Perriard E, Perriard JC, Larsen T, Pedrazzini T, Krek W. Activation of a HIF1alpha-PPARgamma axis underlies the integration of glycolytic and lipid anabolic pathways in pathologic cardiac hypertrophy. *Cell Metab*. 2009;9:512–524. doi: 10.1016/j.cmet.2009.05.005.
9. Battiprolu PK, Hojayev B, Jiang N, Wang ZV, Luo X, Iglewski M, Shelton JM, Gerard RD, Rothermel BA, Gillette TG, Lavandero S, Hill JA. Metabolic stress-induced activation of FoxO1 triggers diabetic cardiomyopathy in mice. *J Clin Invest*. 2012;122:1109–1118. doi: 10.1172/JCI60329.
10. Altin SE, Schulze PC. Metabolism of the right ventricle and the response to hypertrophy and failure. *Prog Cardiovasc Dis*. 2012;55:229–233. doi: 10.1016/j.pcad.2012.07.010.
11. Abel ED, O'Shea KM, Ramasamy R. Insulin resistance: metabolic mechanisms and consequences in the heart. *Arterioscler Thromb Vasc Biol*. 2012;32:2068–2076. doi: 10.1161/ATVBAHA.111.241984.
12. Rider OJ, Cox P, Tyler D, Clarke K, Neubauer S. Myocardial substrate metabolism in obesity. *Int J Obes (Lond)*. 2013;37:972–979. doi: 10.1038/ijo.2012.170.
13. Glatz JF, Luiken JJ, Bonen A. Membrane fatty acid transporters as regulators of lipid metabolism: implications for metabolic disease. *Physiol Rev*. 2010;90:367–417. doi: 10.1152/physrev.00003.2009.
14. Hagberg C, Mehlem A, Falkevall A, Muhl L, Eriksson U. Endothelial fatty acid transport: role of vascular endothelial growth factor B. *Physiology (Bethesda)*. 2013;28:125–134. doi: 10.1152/physiol.00042.2012.
15. Irie H, Krukenkamp IB, Brinkmann JF, Gaudette GR, Saltman AE, Jou W, Glatz JF, Abumrad NA, Ibrahimi A. Myocardial recovery from ischemia is impaired in CD36-null mice and restored by myocyte CD36 expression or medium-chain fatty acids. *Proc Natl Acad Sci U S A*. 2003;100:6819–6824. doi: 10.1073/pnas.1132094100.
16. van der Vusse GJ, van Bilsen M, Glatz JF. Cardiac fatty acid uptake and transport in health and disease. *Cardiovasc Res*. 2000;45:279–293.
17. Binas B, Danneberg H, McWhir J, Mullins L, Clark AJ. Requirement for the heart-type fatty acid binding protein in cardiac fatty acid utilization. *FASEB J*. 1999;13:805–812.
18. Steinbusch LK, Luiken JJ, Vlasblom R, Chabowski A, Hoebers NT, Coumans WA, Vroegrijk IO, Voshol PJ, Ouwens DM, Glatz JF, Diamant M. Absence of fatty acid transporter CD36 protects against Western-type diet-related cardiac dysfunction following pressure overload in mice. *Am J Physiol Endocrinol Metab*. 2011;301:E618–E627. doi: 10.1152/ajpendo.00106.2011.
19. Watanabe K, Ohta Y, Toba K, Ogawa Y, Hanawa H, Hirokawa Y, Kodama M, Tanabe N, Hirono S, Ohkura Y, Nakamura Y, Kato K, Aizawa Y, Fuse I, Miyajima S, Kusano Y, Nagamoto T, Hasegawa G, Naito M. Myocardial CD36 expression and fatty acid accumulation in patients with type I and II CD36 deficiency. *Ann Nucl Med*. 1998;12:261–266.
20. Heather LC, Cole MA, Lygate CA, Evans RD, Stuckey DJ, Murray AJ, Neubauer S, Clarke K. Fatty acid transporter levels and palmitate oxidation rate correlate with ejection fraction in the infarcted rat heart. *Cardiovasc Res*. 2006;72:430–437. doi: 10.1016/j.cardiores.2006.08.020.
21. Hagberg CE, Falkevall A, Wang X, Larsson E, Huusko J, Nilsson I, van Meeteren LA, Samen E, Lu L, Vanwildemeersch M, Klar J, Genove G, Pietras K, Stone-Elander S, Claesson-Welsh L, Ylä-Herttuala S, Lindahl P, Eriksson U. Vascular endothelial growth factor B controls endothelial fatty acid uptake. *Nature*. 2010;464:917–921. doi: 10.1038/nature08945.
22. Hagberg CE, Mehlem A, Falkevall A, Muhl L, Fam BC, Ortsäter H, Scotney P, Nyqvist D, Samén E, Lu L, Stone-Elander S, Proietto J, Andrikopoulos S, Sjöholm A, Nash A, Eriksson U. Targeting VEGF-B as a novel treatment for insulin resistance and type 2 diabetes. *Nature*. 2012;490:426–430. doi: 10.1038/nature11464.

23. Kanda T, Brown JD, Orasanu G, Vogel S, Gonzalez FJ, Sartoretto J, Michel T, Plutzky J. PPARgamma in the endothelium regulates metabolic responses to high-fat diet in mice. *J Clin Invest*. 2009;119:110–124. doi: 10.1172/JCI36233.

24. Burgess R, Rawls A, Brown D, Bradley A, Olson EN. Requirement of the paraxis gene for somite formation and musculoskeletal patterning. *Nature*. 1996;384:570–573. doi: 10.1038/384570a0.

25. Mankoo BS, Collins NS, Ashby P, Grigorieva E, Pevny LH, Candia A, Wright CV, Rigby PW, Pachnis V. Mox2 is a component of the genetic hierarchy controlling limb muscle development. *Nature*. 1999;400:69–73. doi: 10.1038/21892.

26. Burgess R, Cserjesi P, Ligon KL, Olson EN. Paraxis: a basic helix-loop-helix protein expressed in paraxial mesoderm and developing somites. *Dev Biol*. 1995;168:296–306. doi: 10.1006/dbio.1995.1081.

27. Gorski DH, Leal AJ. Inhibition of endothelial cell activation by the homeobox gene Gax. *J Surg Res*. 2003;111:91–99.

28. Wu Z, Guo H, Chow N, Sallstrom J, Bell RD, Deane R, Brooks AI, Kanagala S, Rubio A, Sagare A, Liu D, Li F, Armstrong D, Gasiewicz T, Zidovetzki R, Song X, Hofman F, Zlokovic BV. Role of the MEOX2 homeobox gene in neurovascular dysfunction in Alzheimer disease. *Nat Med*. 2005;11:959–965. doi: 10.1038/nm1287.

29. Quertermous EE, Hidai H, Blanar MA, Quertermous T. Cloning and characterization of a basic helix-loop-helix protein expressed in early mesoderm and the developing somites. *Proc Natl Acad Sci USA*. 1994;91:7066–7070.

30. Aranguren XL, Beerens M, Coppiello G, Wiese C, Vandersmissen I, Nigro AL, Verfaillie CM, Gessler M, Luttun A. COUP-TFII orchestrates venous and lymphatic endothelial identity by homo- or heterodimerisation with PROX1. *J Cell Sci*.2013;126:1164–1175.

31. Calabria AR, Shusta EV. A genomic comparison of *in vivo* and *in vitro* brain microvascular endothelial cells. *J Cereb Blood Flow Metab*. 2008;28:135–148. doi: 10.1038/sj.jcbfm.9600518.

32. Aranguren XL, Agirre X, Beerens M, Coppiello G, Uriz M, Vandersmissen I, Benkheil M, Panadero J, Aguado N, Pascual-Montano A, Segura V, Prósper F, Luttun A. Unraveling a novel transcription factor code determining the human arterial-specific endothelial cell signature. *Blood*. 2013;122:3982–3992. doi: 10.1182/blood-2013-02-483255.

33. Iso T, Maeda K, Hanaoka H, Suga T, Goto K, Syamsunarno MR, Hishiki T, Nagahata Y, Matsui H, Arai M, Yamaguchi A, Abumrad NA, Sano M, Suematsu M, Endo K, Hotamisligil GS, Kurabayashi M. Capillary endothelial fatty acid binding proteins 4 and 5 play a critical role in fatty acid uptake in heart and skeletal muscle. *Arterioscler Thromb Vasc Biol*. 2013;33:2549–2557. doi: 10.1161/ATVBAHA.113.301588.

34. Davies BS, Beigneux AP, Fong LG, Young SG. New wrinkles in lipoprotein lipase biology. *Curr Opin Lipidol*. 2012;23:35–42. doi: 10.1097/MOL.0b013e32834d0b33.

35. Bharadwaj KG, Hiyama Y, Hu Y, Huggins LA, Ramakrishnan R, Abumrad NA, Shulman GI, Blaner WS, Goldberg IJ. Chylomicron- and VLDL-derived lipids enter the heart through different pathways: *in vivo* evidence for receptor- and non-receptor-mediated fatty acid uptake. *J Biol Chem*. 2010;285:37976–37986. doi: 10.1074/jbc.M110.174458.

36. Augustus AS, Buchanan J, Park TS, Hirata K, Noh HL, Sun J, Homma S, D'armiento J, Abel ED, Goldberg IJ. Loss of lipoprotein lipase-derived fatty acids leads to increased cardiac glucose metabolism and heart dysfunction. *J Biol Chem*. 2006;281:8716–8723. doi: 10.1074/jbc.M509890200.

37. van Bilsen M, van Nieuwenhoven FA, van der Vusse GJ. Metabolic remodelling of the failing heart: beneficial or detrimental? *Cardiovasc Res*. 2009;81:420–428. doi: 10.1093/cvr/cvn282.

38. Koskivirta I, Kassiri Z, Rahkonen O, Kiviranta R, Oudit GY, McKee TD, Kytö V, Saraste A, Jokinen E, Liu PP, Vuorio E, Khokha R. Mice with tissue inhibitor of metalloproteinases 4 (Timp4) deletion succumb to induced myocardial infarction but not to cardiac pressure overload. *J Biol Chem*. 2010;285:24487–24493. doi: 10.1074/jbc.M110.136820.

39. Kern CB, Wessels A, McGarity J, Dixon LJ, Alston E, Argraves WS, Geeting D, Nelson CM, Menick DR, Apte SS. Reduced versican cleavage due to Adamts9 haploinsufficiency is associated with cardiac and aortic anomalies. *Matrix Biol*. 2010;29:304–316. doi: 10.1016/j.matbio.2010.01.005.

CLINICAL PERSPECTIVE

Endothelial cells lining capillaries of different organs have specialized gene expression patterns, morphologies, and functions in relation to the specific needs of the tissue parenchymal cells with which they communicate. This microvascular endothelial heterogeneity is determined by environmental cues and intrinsic regulators (eg, transcription factors), many of which remain largely unknown. Furthermore, unlike for liver or brain, information on the specific characteristics of endothelial cells in the heart is currently lacking. Understanding these characteristics and the mechanisms that determine them may form the basis of new therapeutic strategies to tackle heart disease. Here, we identified Meox2 and Tcf15 as transcriptional codeterminants of the heart endothelial gene signature that program the heart endothelium for fatty acid uptake and transport to the heart parenchyma. Combined heterozygous deficiency for these transcription factors resulted in reduced fatty acid uptake and a compensatory increase in glucose uptake in the heart. Because there are many forms of cardiac dysfunction related to changes in energy substrate usage, our insights could be used to develop new strategies based on endothelial Meox2/Tcf15 targeting to treat such dysfunction.

SUPPLEMENTAL MATERIAL

I. EXPANDED METHODS AND RESULTS

A. Extended Methods

Animals and human biopsies. *Tie2-GFP* mice[1] were used as EC donors for expression profiling. *Meox2*^{+/-}*:Tcf15*^{+/-} mice were obtained by intercrossing *Meox2*[Cre/+] (C57Bl/6 background; further referred to as '*Meox2*^{+/-}'; Jackson Laboratories; stockN°003755) and *Tcf15*^{+/-} mice (129S7/SvEvBrd*C57Bl/6 background; provided by E.N. Olson and A. Rawls, Dallas, TX and Tempe, AZ, USA)[2]. After obtaining informed consent, human ECs were isolated from heart biopsies (right atrial appendage from patients undergoing mitral valve surgery without pulmonary hypertension or right heart failure), brain biopsies (cortical tissue from epileptic patients undergoing amygdalo-hippocampectomy) or liver biopsies (patients undergoing elective cholecystectomy). Experimental procedures with animals and human-derived samples were approved by the Ethics Committee on Animal Use of KU Leuven and of University Hospitals Leuven, respectively. Human samples were handled according to the Helsinki Declaration.

EC isolation and culture. For murine microvascular EC isolation, tissues from 8-12 weeks-old mice were dissected out, surrounding connective tissue and visible large vessels removed and tissues enzymatically digested using optimized procedures for each organ (*i.e.*, 1.2 U/ml dispase [BD], followed by Percoll gradient centrifugation for liver; 0.7 mg/ml crude collagenase [Gibco] + 39 U/ml DNAse I [Ambion] followed by bovine serum albumin (BSA) density gradient centrifugation for brain; 0.7 mg/ml crude collagenase for kidney, lung and pancreas; and 1.5 mg/ml collagenase I [Gibco] for heart, skeletal muscle, BAT and WAT). After a final wash in PBS, cells were resuspended in FACS buffer (PBS/EDTA, 1 mM/HEPES, 25 mM/1% BSA, pH7), filtered with a 40 μm mesh and sorted directly in RLT (Qiagen) or TRIzol® (+ 1% β-mercapto-ethanol [BME]) for RNA extraction or in PBS for being washed, pelleted and subsequently resuspended in Gey's buffer for protein extraction or resuspended in incubation medium for *ex vivo* fatty acid (FA) uptake experiments. For profiling, sorting of ~10[6] cells was done with FACS (Area I, BD), based on the GFP[+] fraction from *Tie2-GFP* donors and for each organ, samples were a mix of male and female in a 1:1 ratio. For assaying gene expression in *Meox2*^{+/-}*:Tcf15*^{+/-} donors and their single-heterozygous or wild-type littermates, FACS sorting was based on the CD31^{+}CD34^{+}CD45^{-} fraction and either males or females were used. For *ex vivo* FA uptake experiments and for protein extraction, cells were sorted from *Meox2*^{+/-}*:Tcf15*^{+/-} and wild-type mice by magnetic beads selection (Miltenyi), using a combination of CD102 and CD31

antibodies, after CD45 depletion. Antibodies used for magnetic selection are listed in Supplementary Table I. For human heart ECs, epicardial tissue was removed and biopsies were digested with 1.5 mg/ml collagenase I; for human liver ECs, biopsies were digested with 0.08 Wunsch U/ml liberase (Roche) and 39 U/ml DNAse I; for human brain ECs, meninges and the most external layer of white matter were removed and biopsies were digested with 0.7 mg/ml crude collagenase and 39 U/ml DNAse I followed by BSA density gradient centrifugation. After a final wash in PBS, cells were resuspended in FACS buffer, filtered with a 40 μm mesh and sorted directly in RLT or TRIzol® (+ 1% BME) for RNA extraction. Sorting was done either based on the Tie2^{+}podoplanin^{-}CD45^{-} or the CD31^{+}CD34^{+}CD45^{-} fraction. An antibody list for FACS is provided in Supplementary Table I. To obtain cultured human heart ECs, all cells obtained from freshly digested biopsies were grown on plates coated with 0.1% gelatin in EBM2 medium supplemented with EGM2-MV bullet kit (Lonza) in standard conditions (95% O_2/5% CO_2/37°C). When confluent (after 10-15 days), the Tie2^{+}podoplanin^{-}CD45^{-} or CD31[+](Tie2^{+})CD45^{-} fraction was sorted and re-plated ('passage (P)1') and propagated up to P10. Cells between P1-10 were used for expression profiling of the heart EC signature by qRT-PCR or for lentiviral transduction of heart EC transcription factors (TFs) as described below. Before every experiment cell purity was assessed by CD31 FACS staining. HUVECs were isolated as described[3] and grown in EBM2 medium supplemented with EGM2-MV bullet kit (Lonza) in standard conditions (95% O_2/5% CO_2/37°C).

Microarray analysis. Organs of several 8-12 weeks-old mice (with a 1:1 gender ratio) were pooled to obtain ~10^6 cells per sample in RLT lysis buffer (Qiagen). 10^5 cells from the eGFP[-] non-EC fraction were also sorted. RNA extraction was performed with a Qiagen micro-kit according to the manufacturer's instructions. The VIB Nucleomics Core lab performed the RNA quality control using a Bioanalyzer 2100 (Agilent Technologies) and 500 pg of RNA from the EC fraction of 5 selected samples per tissue was amplified, biotin-labeled and run on a mouse genome-wide microarray (Affymetrics Mo Gene1-0ST). Qualitative and statistical analysis of the microarray output was performed by the Nucleomics Core lab. Statistical analysis was performed using the Lima Package by contrast analysis with a moderated *t*-statistic corrected for multiple testing with Benjamini-Hochberg. For validation, only genes with an absolute Log_2 probe set intensity≥6 and presenting a minimal difference between tissues of 2 Log_2 probe set intensity (corresponding to a 4-fold or higher difference; *P*<0.05) were retained. Microarray data is accessible at the NCBI Gene Expression Omnibus website

(http://www.ncbi.nlm.nih.gov/geo/), accession number GSE48209. Functional annotation analysis was done on the validated gene list with DAVID software (http://david.abcc.ncifcrf.gov/).

Cardiomyocyte isolation and culture. Single ventricular myocytes were enzymatically dissociated from 3- to 4-months-old mice. Mice were injected i.p. with heparin, anesthetized with pentobarbital, and the heart was quickly excised. After cannulation of the aorta, hearts were mounted on a Langendorff perfusion set. The heart was briefly rinsed with normal Tyrode solution, containing 137 mM NaCl, 5.4 mM KCl, 0.5 mM $MgCl_2$, 1 mM $CaCl_2$, 11.8 mM Hepes, 10 mM glucose and 10 mM 2,3-butanedione monoxime (BDM; Sigma Aldrich), pH adjusted to 7.4 with NaOH. Subsequently it was perfused with a Ca^{2+}-free Tyrode solution for 10 minutes. The Ca^{2+}-free Tyrode solution contained 130 mM NaCl, 5.4 mM KCl, 1.2 mM KH_2PO_4, 1.2 mM $MgSO_4$, 6 mM Hepes, 20 mM glucose and 10 mM BDM, pH adjusted to 7.2 with NaOH. Collagenase type II 672 U/ml (Worthington), and 30 μM $CaCl_2$ added to the Ca^{2+}-free Tyrode solution, were recirculated for 8-10 minutes. The enzymes were washed out with low Ca^{2+} Tyrode solution, *i.e.*, the Ca^{2+}-free solution to which 0.18 mM $CaCl_2$ was added, supplemented with 0.5% BSA (Sigma) for 3 minutes and then again with low Ca^{2+} Tyrode solution without BSA for 3 minutes. All solutions used were continuously gassed with 95% O_2/5% CO_2. The heart was then removed from the perfusion apparatus, the ventricles dissociated into single cells by pipetting and afterwards with 5 minutes gentle shaking. Cells were sieved through a 250 μm mesh opening, washed twice with Ca^{2+}-free Tyrode solution supplemented with increasing doses of Ca^{2+} (0.5 and 1 mM) and pelleted by centrifugation at 50g for 1 minute after each wash. Finally, cardiomyocytes were collected in TRIzol® or RIPA buffer for *ex-vivo* qRT-PCR or Western blot analysis, or resuspended in culture medium (M199 medium, Gibco-Life Technologies), supplemented with 2 mM carnitine, 5 mM taurine, 5 mM creatine (all Sigma Aldrich), and 10 mM BDM, plated onto dishes previously coated with laminin (Sigma Aldrich), and allowed to attach for four hours under standard conditions (95% O_2/5% CO_2, 37°C) before using them for *in vitro* FA uptake experiments.

RNA/protein isolation, cDNA preparation, qRT-PCR and Western blot. RNA isolation, qRT-PCR and Western blot were performed as described[3]. Briefly, total RNA from cell lysates was extracted using TRIzol® reagent (Invitrogen) or RLT lysis buffer (Qiagen). mRNA was reverse transcribed using Superscript III Reverse Transcriptase (Invitrogen) and cDNA underwent 40 rounds of amplification on an ABI PRISM 7700 cycler (Applied Biosystems) for standard SYBR-Green (Applied Biosystems) qRT-PCR. Primer sequences are listed in Supplementary Table 2. mRNA levels were normalized using

Gapdh, *Actb* or *Tubb* as housekeeping gene. For copy number quantification of gene expression between different cell types, the same amount of RNA was retro-transcribed and copy number was expressed relative to housekeeping gene copy number (*Gapdh*). Proteins were extracted with RIPA buffer (Sigma) supplemented with protease inhibitors. For Western blotting, 10 to 40 μg of protein was used. Blot pictures were recorded with a Bio-Rad Chemidoc XRS+ molecular imager, equipped with Image Lab software (Bio-Rad laboratories). An antibody list for Western blotting is provided in Supplementary Table I.

Lentiviral overexpression. Virus productions were titered to use the minimum amount of virus giving ~100% transduction. For transduction, 25,000 cultured human heart ECs were plated on 0.1% gelatin-coated 24-well plates, in the morning and transduced in the evening. The medium was changed 12 hours post-transduction. When multiple transductions were performed, the different viruses were added with an interval of 24 hours. Cells were seeded at day 1 in the morning and viruses were added on a fixed day, *i.e.*, *Tcf15*-overexpressing lentivirus was added at day 1 in the evening, *MEOX2* lentivirus at day 2, *PPARG* lentivirus at day 3 and *WT1* lentivirus at day 4. For all conditions, cells were lysed at day 7 for RNA extraction, cDNA synthesis and qRT-PCR analysis or Western blot experiments.

***siRNA* knockdown.** *siRNA* knockdown was performed using *Silencer®* Select pre-designed *siRNA* from Applied Biosystems for *LPL* (*siRNA* ID#: s701); *CD36* (*siRNA* ID# s2645) and non-silencing *negative control 1* ('*NS*'; *siRNA* ID#: am4636). Briefly, 3 days after lentiviral transduction, 10,000 heart ECs were plated on 1.9 cm^2 wells (= day 0). On day 1, cells were transfected by adding to the growth medium 5 pmol *siRNA* mixed with 0.5 μl of Lipofectamine 2000 (Life Technologies,) in 100 μl of OPTI-MEM (Life Technologies). The day after, transfection media was replaced and cells were maintained until day 4. In all cases *siRNA NS*-transfected cells were used as reference. Knockdown efficiency was tested by qRT-PCR and was 90% for *CD36* and 93% for *LPL*.

***In vitro* and *ex vivo* FA uptake.** Cultured human heart ECs 72 hours post-transduction or after *siRNA* treatment or freshly isolated magnetically selected murine heart ECs were incubated with QBT reagent (BODIPY-labeled dodecanoic acid coupled to a quenching element; Molecular Devices) in HBSS buffer + 0.1% FA-free BSA for 30 minutes to determine free FA uptake. For VLDL-derived FA uptake, cells were incubated with 10 μg/ml DiI-Human VLDL (Kalen Biomedical) for 2 hours in Gey's buffer. Before FACS analysis, cultured cells were washed and harvested. Resuspended cells were washed with

PBS several times, pelleted and fixed with 0.4% PFA in PBS. For free FA uptake in cardiomyocytes, BODIPY-PA (Molecular Probes) was used and fixed cells counterstained with DAPI were photographed on a Zeiss Axiovert 200M microscope equipped with a Zeiss MRc5 camera and Axiovision 4.8 software.

***In vitro* FA transport transwell assay.** FA transport was analyzed in cultured HUVECs. Seventy-two hours post-transduction 50,000 HUVECs overexpressing *MEOX2+Tcf15* or a Cherry reporter were seeded on 24-well transwell inserts (0.4 μm pore size; Corning). The day after, medium was changed to M199 (Gibco) supplemented with 20% fetal bovine serum (FBS), 2 mM L-glutamine, 30 mg/L EC growth factor supplements (EGCS), 10 units/ml heparin, 50 IU/ml penicillin and 50 mg/ml streptomycin. After 3 days, 0.05 μCi/well ^{14}C-Palmitic acid (PerkinElmer) and 0.75 μg/ml Texas-Red Dextran (MW 70,000; Invitrogen) was added to the apical chamber. Eight minutes later, the entire lower liquid compartment was collected and used as sample for time zero. Thereafter, 50 μl samples were collected from the lower compartment at 30 minutes, 1 hour, 2, 4 and 6 hours and replaced with 50 μl of medium. For quantification of Dextran fluorescence, samples were measured with a fluorescence reader. For measurement of the ^{14}C signal, samples were suspended in Emulsifier Safe Liquid Scintillation Cocktail (PerkinElmer) and total radioactivity was measured by liquid scintillation counting. Each experiment was performed in quadruplicate.

***In vitro* FA transport co-culture.** 50,000 HUVECs transduced with *Cherry* or *MEOX2+Tcf15* were resuspended in EGM2-MV and applied on the bottom side of the membrane of an inverted transwell column (Corning). Cells were maintained in this position for 30 minutes at 37ºC to allow attachment to the membrane. Next, the transwell column was introduced with the cells in downward position in a 24-well plate containing EGM2-MV and cultured overnight at 37ºC, 5% CO_2. The next day, HUVECs were washed with Gey's buffer and incubated for 1 hour with 0.5 μCi/well of ^{14}C-Oleic Acid (OA; Perkin Elmer) in Gey's buffer + 0.1% FA-free BSA. Thereafter, HUVEC monolayers were extensively washed (5 times for 2-3 minutes) with Gey's buffer and the transwell column was transferred to a 24-well plate containing primary rat cardiomyocytes (Lonza). The co-culture was incubated in cardiomyocyte medium (Lonza) for 6 hours at 37ºC to allow the transfer of ^{14}C-OA from ECs to the cardiomyocytes. Next, the transwell column was removed and cardiomyocytes were thoroughly washed with PBS containing Ca^{2+} and Mg^{2+} (3 times for 2 minutes) and lysed with PBS + 1% Triton

for 5 minutes. Cell lysates were resuspended in Emulsifier Safe Liquid Scintillation Cocktail (PerkinElmer) and total radioactivity was measured by liquid scintillation counting.

LPL protein and activity quantification. For quantification on tissues, whole hearts were isolated from $Meox2^{+/-}:Tcf15^{+/-}$ and wild-type mice anesthetized by i.p. injection of a ketamine (100 mg/kg) and xylazine (10 mg/kg) mixture and perfused through the heart apex with 0.9% saline solution to completely remove the blood. Hearts were snap-frozen in liquid N_2 and stored at -80°C until analysis. Frozen hearts were homogenized by shaking (using a Ribolyser) in 300 μl of PBS containing protease inhibitors and lysing matrix D (MP Biomedicals). Cleared supernatants were used for protein quantification and for LPL ELISA (Cusabio) and LPL activity measurement (Roar) according to the manufacturer's instructions. For quantification of LPL activity on cultured cells, cell monolayers were thoroughly washed in PBS, trypsinized, washed again in PBS and collected in 100 μl PBS containing protease inhibitors. LPL quantity and activity were normalized for protein content.

Proximity ligation assay (PLA). PLA was performed using the DuolinkII PLA kit (Sigma) as described[4]. To test Meox2 and Tcf15 heterodimerization, HUVECs were transduced with lentiviruses encoding MEOX2 and FLAG-tagged Tcf15. As negative control, non-transduced cells or cells transduced with MEOX2 and FLAG-tagged PROX1 were used. To determine Meox2-Tcf15 heterodimer formation anti-Meox2 and anti-FLAG antibodies (Supplementary Table 1) were used, followed by Duolink II anti-mouse PLUS (positive oligonucleotide) and Duolink II anti-rabbit MINUS (negative complementary oligonucleotide) secondary antibodies. Duolink II Detection Reagent Orange was used to visualize protein interactions. Confocal images were recorded with a Zeiss LSM510 confocal microscope equipped with LSM510 software (Carl Zeiss).

GST pull-down assay. GST pull-down assay was performed according to the manufacturer's instructions with minor modifications (Pierce GST Protein Interaction Pull Down Kit). Two 10 cm^2 plates were seeded with 5x10^6 HEK293 cells each and transfected with 4 μg of GST-Tcf15 and 4 μg of FLAG-MEOX2 plasmids alone or in combination. When GST-Tcf15 and FLAG-tagged MEOX2 were used alone, 4 μg of Cherry control plasmid was also added. Forty-eight hours after transfection, cells were collected, lysed and incubated on glutathione agarose columns overnight. The next day, unbound proteins were extensively washed, followed by elution of bound proteins with 100 mM glutathione.

Protein interactions were analyzed by Western blot using anti-GST and anti-FLAG antibodies (Supplementary Table I).

Histology. Sirius-red, immunofluorescence and Oil Red-O stainings were performed as described[5,6]. Briefly, for Oil Red-O staining, mice were anesthetized with pentobarbital, hearts were rapidly excised, washed in KCl 1M and PBS, directly snap-frozen in liquid N_2 and conserved at -80°C until used. Frozen hearts were embedded in Tissue-tek freezing medium (Leica Biosystems), cryo-sectioned at 10 μm, air-dried for 10 minutes and immediately stored at -20°C to be used the same day. Tissues were rinsed with milliQ water and fixed for 1 hour with 3.7% formaldehyde in milliQ water. After one rinse in milliQ water, slides were immersed in a freshly prepared, Wattman-filtered Oil Red-O solution (0.3% Oil Red-O in 60% Triethyl-phosphate-H_2O) for 30 minutes, rinsed with milliQ water and deionized water and mounted with Aquadrop (Merck). Immunofluorescence and immunohistochemical stainings were performed on 3-6 μm sections of paraffin embedded tissues. An antibody list for immunofluorescence stainings is provided in Supplementary Table 1. Images were recorded on a Zeiss Axiovert 200M microscope equipped with a Zeiss MRc5 camera and Axiovision 4.8 software. Capillary/cardiomyocyte ratio and cardiomyocyte cross-sectional area were quantified by a blinded investigator on 20-30 pictures per mouse, using Image J software.

***In vivo* FA uptake.** For the assessment of FA uptake *in vivo*, 5 to 14 wild-type and *Meox2^{+/-}:Tcf15^{+/-}* mice were injected intravenously with a 2 μCi dose of [1-^{14}C]-Oleic Acid (^{14}C-OA; PerkinElmer) dissolved in saline (1:4). For the analysis of ^{14}C-OA in tissues, and after 30 minutes of intravenous injection, mice were anesthetized with an i.p. injection of a ketamine (75 mg/kg) and xylazine (10 mg/kg) mixture and perfused with 0.9% saline solution. Plasma was sampled and organs (heart, soleus muscle, liver, brain, brown and white adipose tissue or BAT and WAT, respectively) were dissected, weighed and solubilized by the addition of Solvable (PerkinElmer, 1 ml/100 mg tissue) in a glass scintillation vial and incubated at 60°C overnight. After cooling to room temperature, 30% (w/w) hydrogen peroxide was added followed by heating at 60°C for another hour to minimize color quenching of samples. Finally, scintillation fluid (Normascint, Scharlab) was added to each sample followed by vigorous shaking. The vials were then allowed to equilibrate in the dark for at least 60 minutes before scintillation counting using an LKB-Wallac-Rackbeta-1214 Counter (PerkinElmer). Final data are expressed as % injected dose per gram of tissue. For autoradiography experiments, wild-type and *Meox2^{+/-}:Tcf15^{+/-}* mice (*n*=3 per group) were injected with saline (background control) or 100

μCi [^{3}H]OA and sacrificed by cervical dislocation 30 minutes after injection. Hearts were dissected out and, after removal of the atrial appendages, immersed in KCl 1M. Samples were rinsed in cacodylate buffer (0.1 M + 3 mM CaCl$_2$) and fixed overnight in fixative solution (2% glutaraldehyde + 3 mM CaCl$_2$ in 0.1 M cacodylate buffer, pH 7.4) at 4°C. Ventricles were cut transversally at 200 μm, post-fixed in 2% osmium tetroxide for 2 hours, partially dehydrated and embedded in LBR White at low temperatures (from 0ºC to -4ºC) to avoid loss of lipids during sample preparation. Semi-thin sections (2 μm) were cut with a diamond knife and mounted onto slides, dipped in autoradiographic emulsion (Kodac Autoradiography Emulsion type NTB), exposed for 25 days at 4ºC, developed in G 150 developer (Agfa), and counterstained with 1% toluidine blue.

[^{18}F]FDG PET imaging. Glucose uptake in the heart was measured by positron emission tomography (PET) with the radiotracer 2-deoxy-2-[^{18}F]fluoro-D-glucose ([^{18}F]FDG), synthetized by standard nucleophilic substitution methods at the Clínica Universidad de Navarra PET-GMP laboratory. PET imaging was performed in a dedicated small animal scanner (Philips Mosaic), with 2 mm resolution at full width half maximum (FWHM), 11.9 cm axial field of view (FOV) and 12.8 cm transaxial FOV. Mice (*n*=12 wild-type and *n*=11 *Meox2$^{+/-}$:Tcf15$^{+/-}$*) were anesthetized with 2% isoflurane in 100% O$_2$ gas and placed horizontally on the PET scanner bed. The [^{18}F]FDG (7.9 ± 1.5 MBq in 100 μl saline) was injected through the tail vein simultaneously at the beginning of a list mode study of 60 minutes. For each study, a summed sinogram of the whole emission study and an 18 frame dynamic sinogram (2 ×15"; 7×30"; 1×60"; 1x120"; 1x180"; 2x300"; 4x300") were created. From these sinograms, both a summed and a dynamic image were generated containing the information about the corresponding time intervals. All the images were reconstructed using the 3D Ramla algorithm with 2 iterations and a relaxation parameter of 0.024 into a 128×128 matrix with a 1 mm voxel size applying dead time, decay, random and scattering corrections. For the assessment of [^{18}F]FDG uptake in the heart, all studies were exported and analyzed using the PMOD software (PMOD Technologies Ltd., Adliswil, Switzerland). For each mouse, a volume of interest (VOI) of the heart was drawn on coronal 1 mm-thick slices of summed PET images. Then, VOI was applied to the dynamic image to obtain the [^{18}F]FDG uptake values for each time point. The obtained data were normalized by the specific dose at the time of injection.

B. Supplementary Notes

Supplementary Note I. Microvascular EC purity.

As a source for sorting ECs from the heart, we used *Tie2-GFP* mice in which the *Tie2* promoter-enhancer is active in blood-vascular but not lymphatic ECs[1]. As previously described, CD36 is highly expressed in microvascular ECs and absent in ECs from large vessels[7]. Nevertheless, between capillary ECs from different organs there is a different degree of expression of CD36, being very low in brain ECs and high in liver and heart ECs (ref. 8 and as evident from our microarray analysis; Supplementary Figure VC). Indeed, for heart and liver, microvascular EC purity could be determined by FACS for CD36 (as shown for the heart in Supplementary Figure IA), whereas under identical FACS staining conditions we could not detect CD36 positive cells in brain ECs. Therefore, to confirm microvascular EC purity of brain EC preparations, we relied upon the significant enrichment for known brain-specific microvascular EC markers such as *Glut1*, *Lat1*, *Ocln* and *Tfrc* (Supplementary Figure IC).

Supplementary Note II. Relative abundance of WT1 isoforms in cardiac ECs.

Several WT1 isoforms have been described with different tissue specificities and functions[9]. We quantified the relative abundance of the long *versus* short isoforms (the latter generated from an alternative start codon in intron 1) and of the isoforms carrying or not the KTS domain in freshly isolated human and mouse heart ECs and found that the most abundant WT1 isoform in heart ECs is the isoform expressing exon1 and the KTS domain (ratio isoform - exon1/isoform + exon1 = 1:1,500, and 71 ± 8% carrying the KTS element). We therefore overexpressed the isoform D (expressing exon1, exon5 and carrying KTS), the most prevalent isoform of WT1[(9)] in normal tissues, to test its effect on the heart EC gene signature.

Supplementary Note III. Mendelian ratios of *Meox2*^{+/-} x *Meox2*^{+/-} intercrosses.

Meox2[Cre/+] mice were obtained from the Jackson Laboratories (stockN°003755) and crossed for one additional generation in C57Bl/6 to establish the colony. When setting up *Meox2*[Cre/+] x *Meox2*[Cre/+] crosses to obtain *Meox2*[cre/cre] (or *Meox2*^{-/-}) mice, we observed that *Meox2*^{-/-} pups died within a few hours after birth, while the ratios just before birth (at embryonic day 19.5) were Mendelian. This observation is at variance with what is reported on the Jackson Laboratory website where it is mentioned that *Meox2*^{-/-} mice are viable at birth and die just before weaning (http://jaxmice.jax.org/strain/003755.html).
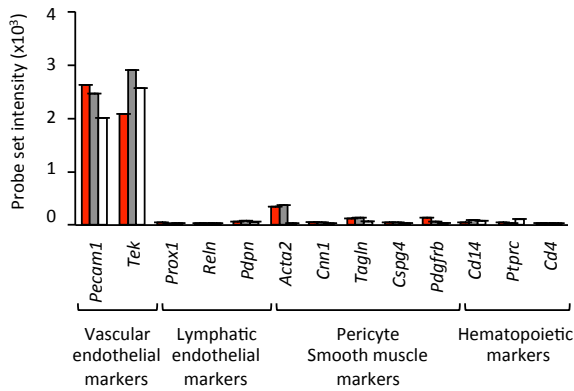
II. SUPPLEMENTARY FIGURES

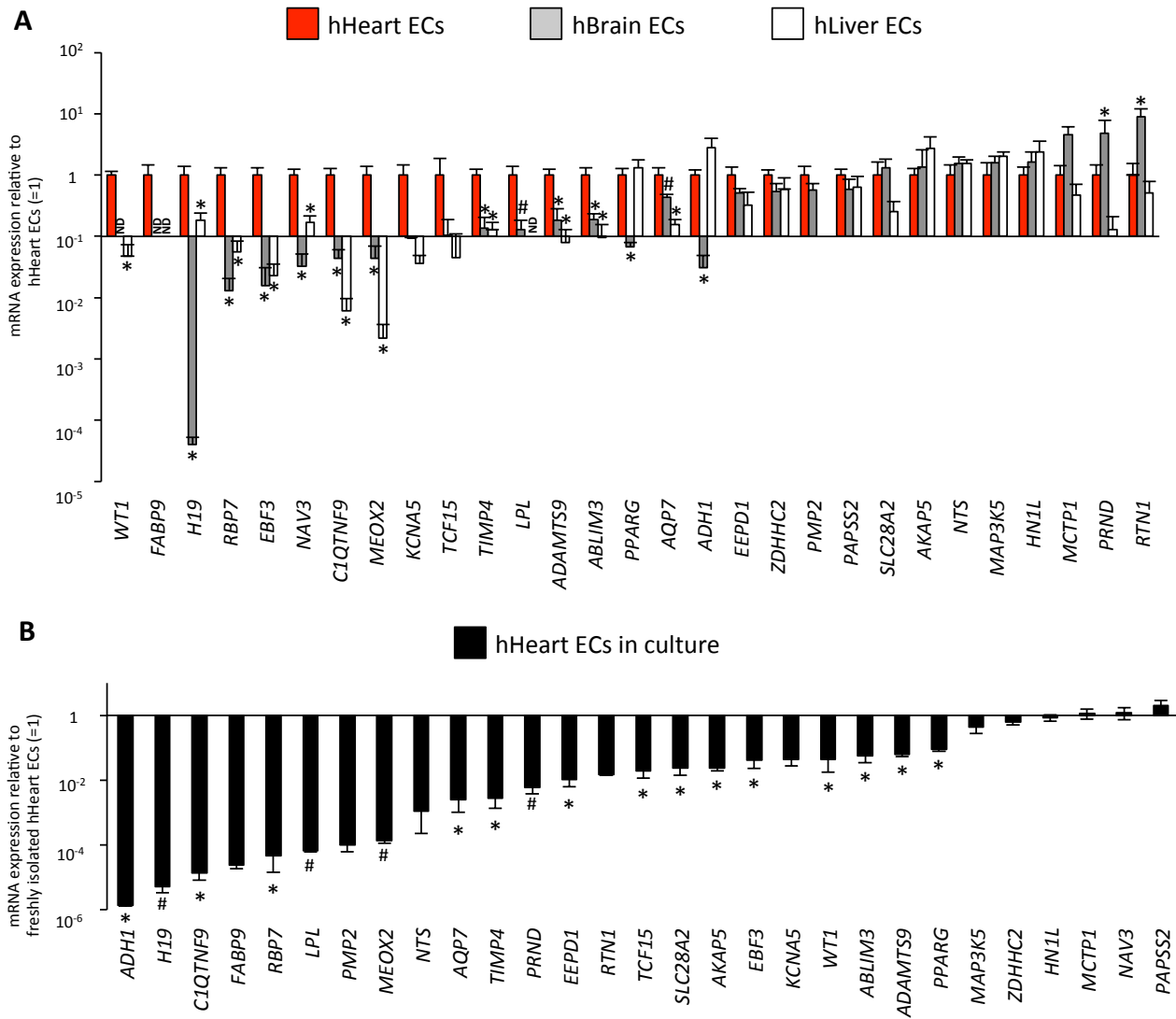**Supplementary Figure I.**
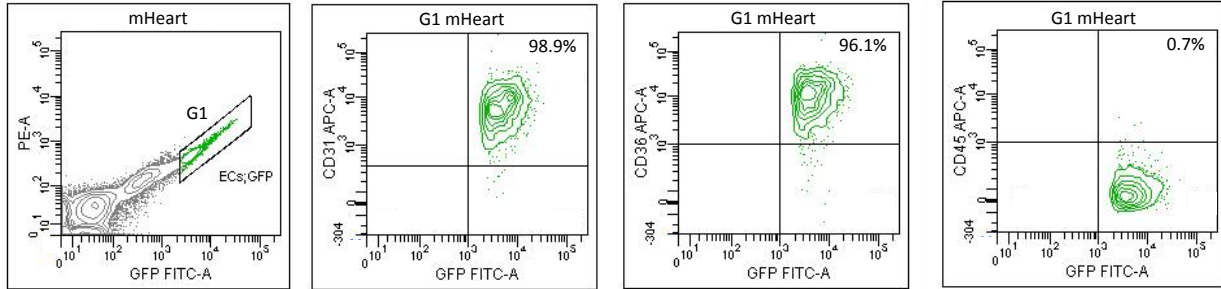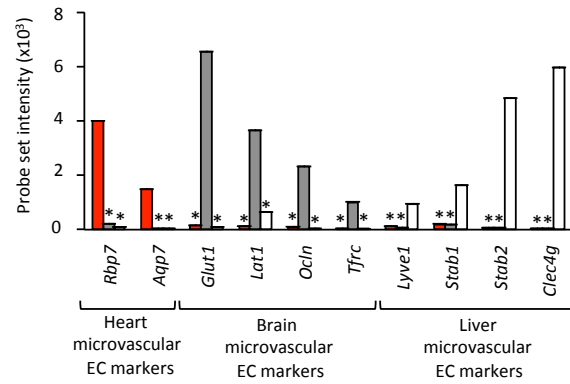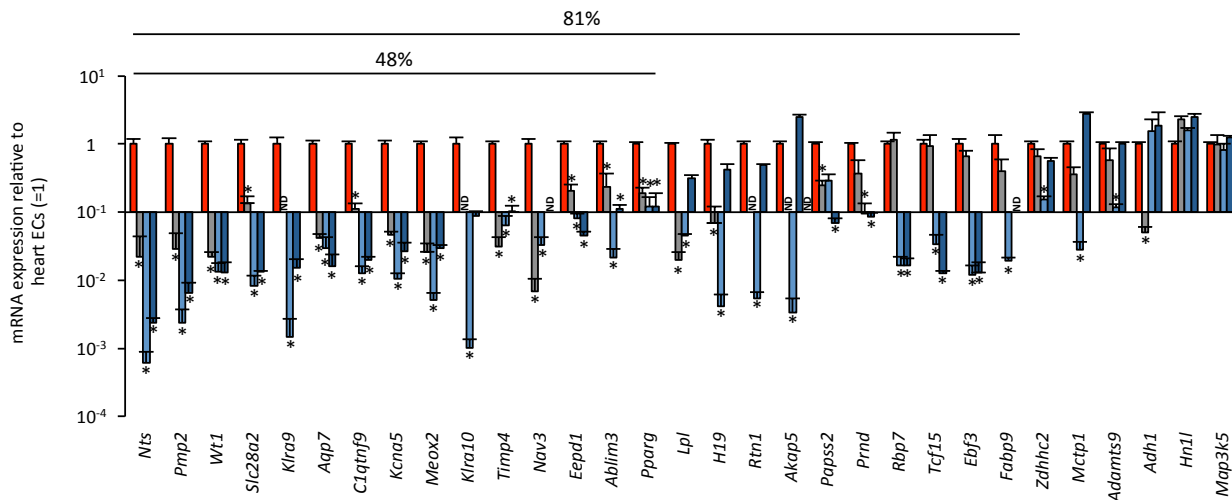
Supplementary Figure I. Sorting strategy and microarray validation.

A, Representative FACS plots of heart homogenates from *Tie2-GFP* mice showing gate (G1) setting for sorting of GFP$^+$ endothelial cells (ECs) and G1 analysis revealing 99% purity for EC marker CD31 and 96% for microvascular EC marker CD36[7], and negligible contamination (<1%) with hematopoietic cells (expressing CD45). **B,** Probe set intensities for heart, brain and liver EC samples for vascular endothelial, lymphatic endothelial, pericyte-smooth muscle or hematopoietic markers demonstrating the purity of the sorted EC fractions used for microarray. **C,** Probe set intensities for heart, brain and liver EC samples for previously described heart, brain and liver-specific microvascular EC markers, demonstrating the expected enrichment of previously known tissue-specific microvascular EC markers in the corresponding tissue EC types[10-13] (*n*=5; *P<0.05 *versus* corresponding specific organ and a minimum 4-fold difference and Log$_2$ probe intensity ≥6). **D,** mRNA expression determined by qRT-PCR of genes of the heart EC fingerprint in heart, pancreas, kidney or lung ECs relative to heart ECs (*n*=3-4; *P<0.05 *versus* heart ECs and a minimum 4-fold difference), revealing that most genes (81% compared to at least 2 of these tissues and 48% compared to all three tissues) were at least 4-fold enriched in heart ECs. ND: not detectable. Quantitative data represent mean ± s.e.m.
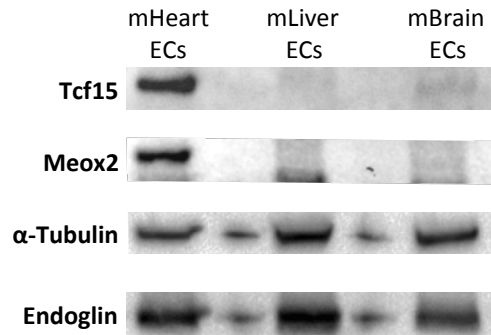
Supplementary Figure II.

Supplementary Figure II. Analysis of the heart EC fingerprint in freshly isolated and cultured human EC samples.

A, mRNA expression determined by qRT-PCR of genes of the heart EC fingerprint in human (h) heart, brain or liver ECs relative to human heart ECs (n=3-10; *P<0.05; #P<0.1 *versus* heart ECs), revealing that part of the signature is also enriched in human heart ECs *versus* brain and liver ECs. ND: not detectable. **B,** mRNA expression determined by qRT-PCR of genes of the heart EC fingerprint in cultured (passage 1-10) human (h) heart ECs relative to freshly isolated human heart ECs (n=3-10; *P<0.05; #P<0.1 *versus* freshly isolated heart ECs), revealing that the majority of the genes of the heart EC fingerprint is silenced at least 90%. Data represent mean ± s.e.m.
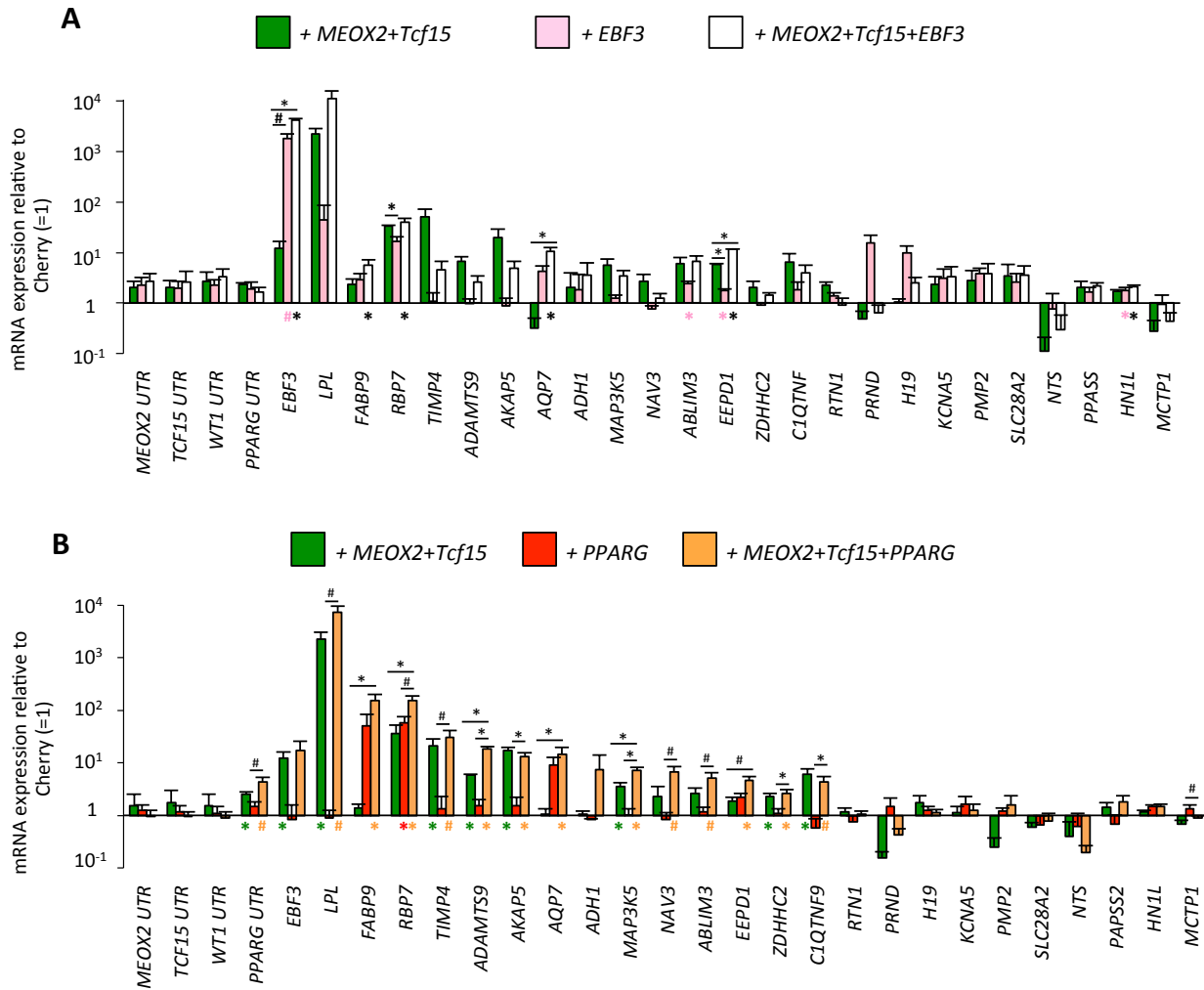
Supplementary Figure III.

Supplementary Figure III. Meox2 and Tcf15 protein expression in murine tissues.

Western blots of Meox2 and Tcf15 expression, housekeeping protein expression (α-Tubulin) and EC marker Endoglin on freshly isolated ECs from murine (m) heart, liver and brain confirm the unique expression of Meox2 and Tcf15 in ECs from the heart.
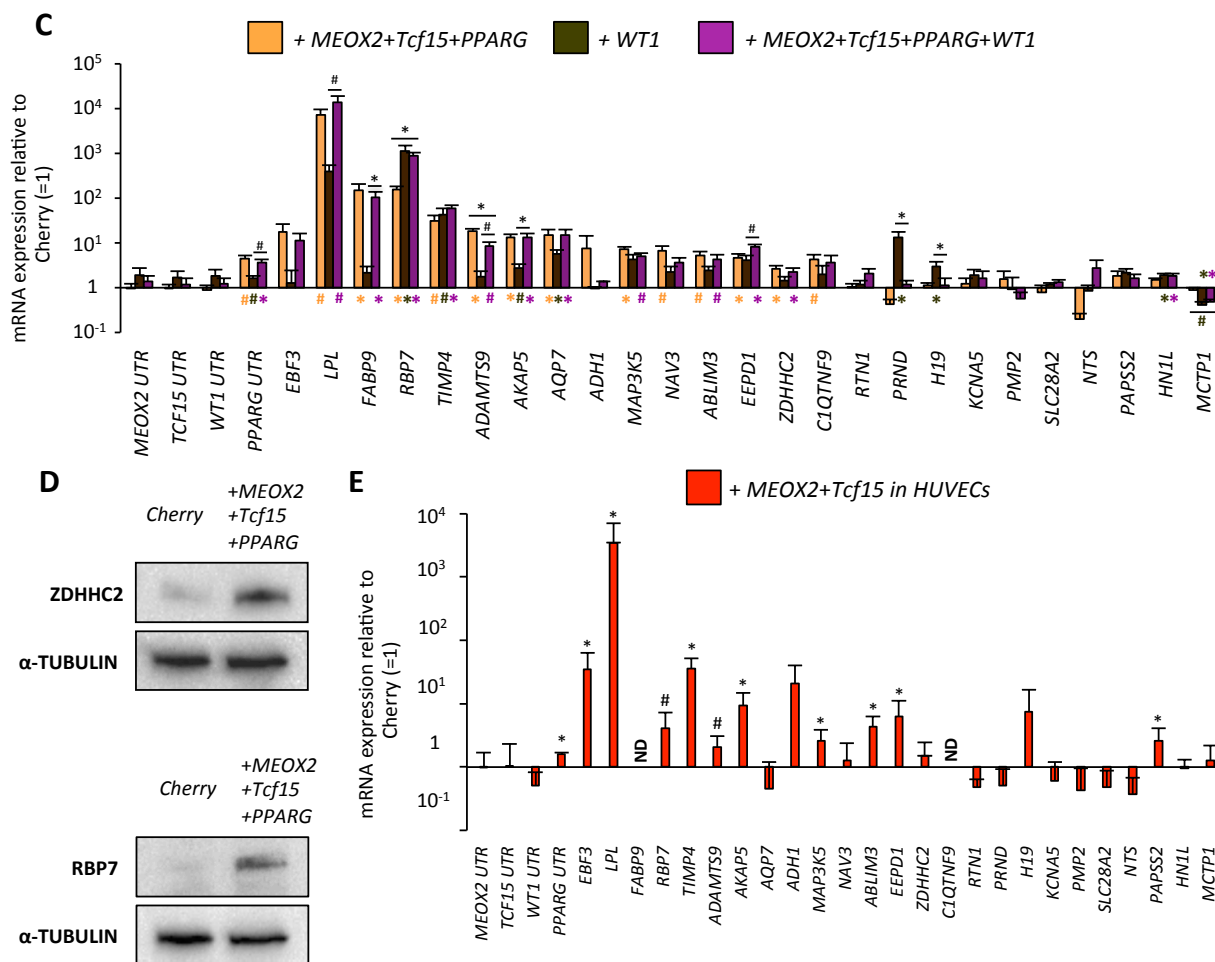
Supplementary Figure IVA,B.

Supplementary Figure IVA,B. Analysis of TF overexpression on the heart EC fingerprint in cultured human heart ECs.

Diagrams represent mRNA expression determined by qRT-PCR for 29 genes of the heart EC fingerprint in cultured human heart ECs overexpressing certain TF (combination)s relative to a 'Cherry' reporter control. Primers in the 3'UTR region were used to distinguish endogenous expression from that caused by lentiviral overexpression. Two of the 31 signature genes were not included, *i.e.*, *Klra9* and *Klra10*, as there is no human equivalent. Data represent mean ± s.e.m. **A,** Overexpression of *MEOX2+Tcf15*, *EBF3* or *MEOX2+Tcf15+EBF3 versus* Cherry (*$P<0.037$ or #$P<0.05$ *versus* Cherry shown under the bars [for *EBF3* or *MEOX2+Tcf15+EBF3*]; or *versus MEOX2+Tcf15* as indicated above the bars; *$P<0.037$ was considered significant [α']; *n*=3-4). **B,** Overexpression of

MEOX2+Tcf15, PPARG or *MEOX2+Tcf15+PPARG versus* Cherry (*P<0.027 or [#]P<0.05 *versus* Cherry shown under the bars; or *versus* another condition as indicated above the bars; *P<0.027 was considered significant [α']; *n*=3-9 independent experiments; for each comparison shown in Supplementary Figure IVB,C and Figure 2A all the conditions were tested and analyzed in parallel; in all experiments where *PPARG* was overexpressed, an agonist, rosiglitazone, was added at 10 μM). When *PPARG* was overexpressed alone, we measured a strong upregulation of three genes, two known targets, *RBP7*[(14)] and *AQP7*[(15)], and one novel target (*FABP9*). When *PPARG* was combined with *MEOX2+Tcf15*, for multiple genes, a superior inductive effect was obtained compared to *MEOX2+Tcf15*.
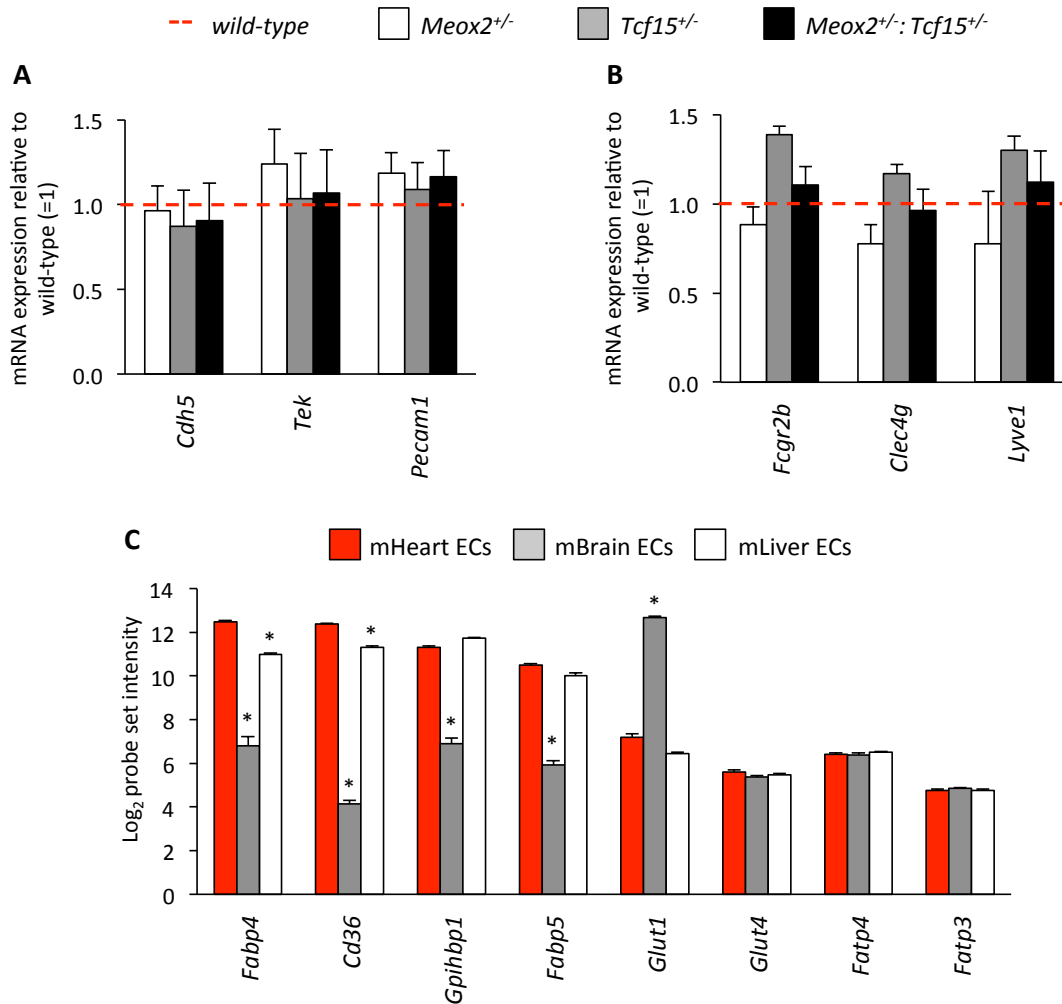
Supplementary Figure IVC-E.

Supplementary Figure IVC-E. Analysis of TF overexpression on the heart EC fingerprint in cultured human ECs.

Diagrams in **C,E** represent mRNA expression determined by qRT-PCR for 29 genes of the heart EC fingerprint in cultured human ECs (heart ECs in panel C, HUVECs in panel E) overexpressing certain transcription factor (combination)s relative to a 'Cherry' reporter control. Primers in the 3'UTR region were used to distinguish endogenous expression from that caused by lentiviral overexpression. Two of the 31 signature genes were not included, *i.e.*, *Klra9* and *Klra10*, as there is no human equivalent. Data represent mean ± s.e.m. **C,** Overexpression of *MEOX2+Tcf15+PPARG*, *WT1* or *MEOX2+Tcf15+PPARG+WT1 versus* Cherry (*$P<0.027$ or #$P<0.05$ *versus* Cherry shown under the bars; or *versus* another condition as indicated above the bars; *$P<0.027$ was considered significant [α'];

n=3-9 independent experiments; for each comparison shown in Supplementary Figure IVB,C and Figure 2A all the conditions were tested and analyzed in parallel). Upon overexpression of *WT1* alone, we detected an upregulation of multiple genes of the signature, however, combining overexpression of *WT1* with *MEOX2/Tcf15/PPARG* did not have an additive effect. **D,** Western blots for ZDHHC2 and RBP7 in cultured human heart ECs transduced with Cherry or *MEOX2+Tcf15+PPARG*. α-TUBULIN was used as loading control. **E,** Overexpression of *MEOX2+Tcf15* in HUVECs. (*n*=3-7; **P<0.05; \#P<0.1 versus* Cherry).
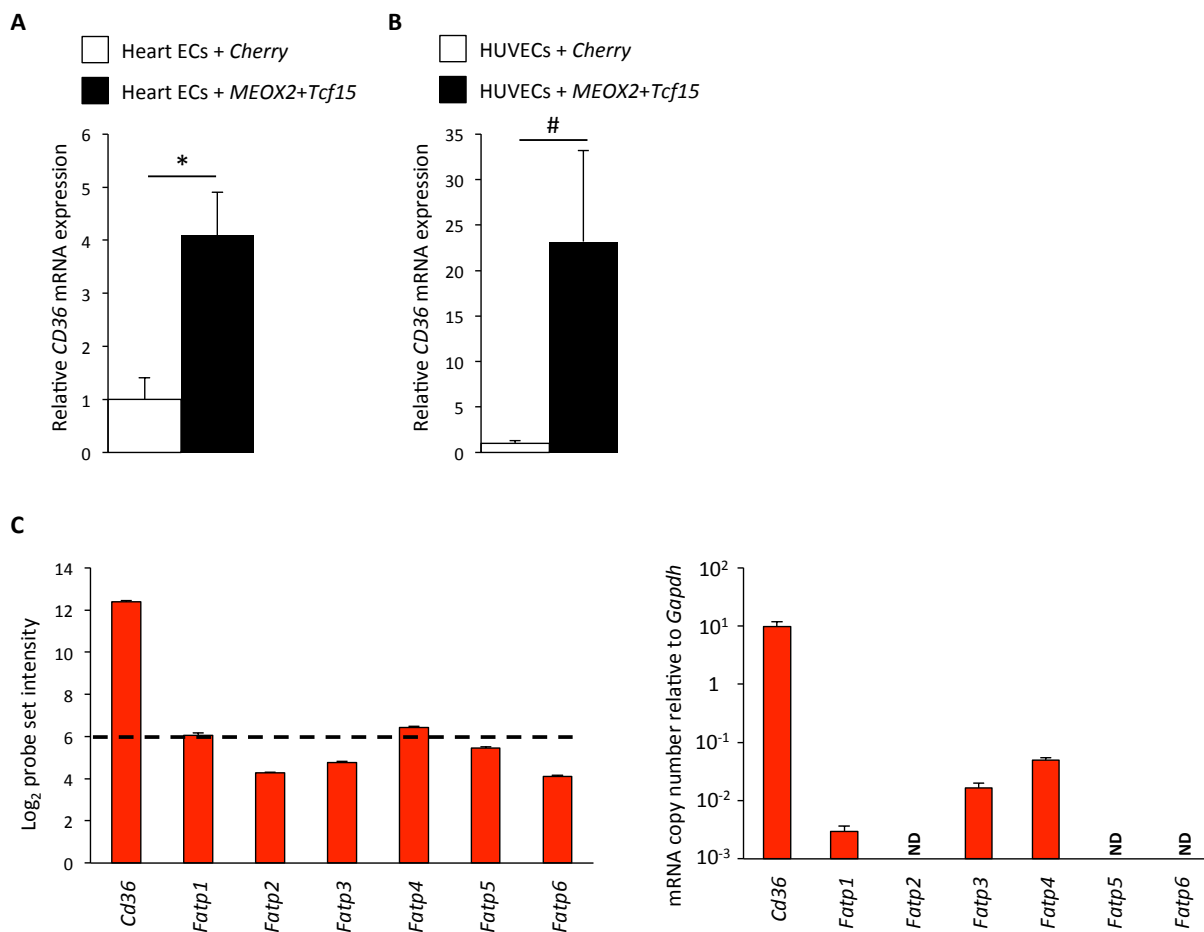
Supplementary Figure V.

Supplementary Figure V. Analysis of genes outside the heart EC fingerprint in *Meox2^{+/-}:Tcf15^{+/-}* mice and freshly isolated ECs.

A, mRNA expression determined by qRT-PCR of general EC markers in heart ECs sorted from *Meox2^{+/-}*, *Tcf15^{+/-}*, or *Meox2^{+/-}:Tcf15^{+/-}* littermates relative to wild-type heart ECs (n=6-8) revealing no significant differences in expression. **B,** mRNA expression determined by qRT-PCR of liver sinusoidal (LS)EC markers in liver ECs sorted from *Meox2^{+/-}*, *Tcf15^{+/-}*, or *Meox2^{+/-}:Tcf15^{+/-}* littermates relative to wild-type LSECs (n=4-8) revealing no significant differences in expression. **C,** Probe set intensities (in Log$_2$ scale) for murine heart, brain and liver EC samples for several genes encoding fatty acid or glucose transport-related molecules. (n=5; *$P<0.05$ *versus* heart ECs). Data represent mean ± s.e.m.
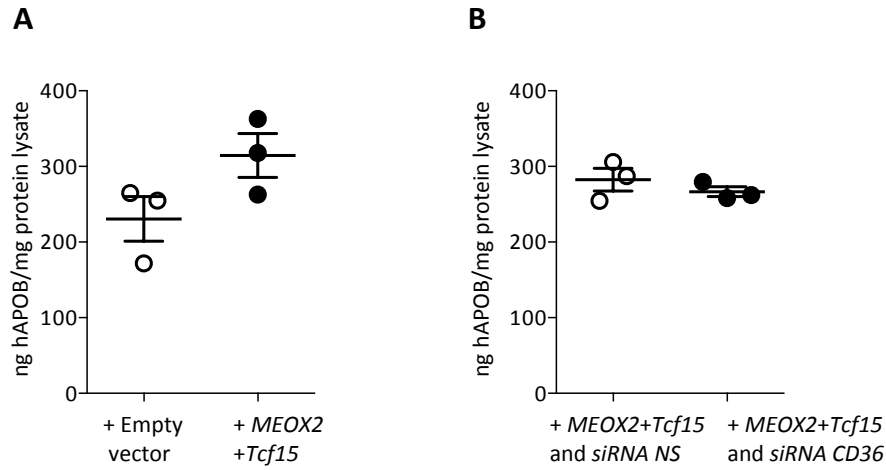
Supplementary Figure VI.

Supplementary Figure VI. CD36 regulation by *MEOX2+Tcf15* and comparative expression analysis of FA transporters in heart ECs.

A,B, Diagram representing qRT-PCR relative quantification of *CD36* in cultured human heart ECs (**A**) and HUVECs (**B**) transduced with *MEOX2+Tcf15 versus* Cherry. (n=5-7; *P<0.05; #P<0.1). **C,** Left: Log_2 microarray probe set intensity for the most described membrane FA translocase/transporters revealing that *CD36* is the FA translocase expressed at the highest level in freshly isolated murine heart ECs (n=5). Right: qRT-PCR copy number quantification relative to *Gapdh* confirming the microarray data on the left (n=4-7). Data represent mean ± s.e.m.

Supplementary Figure VII.

A
B

Supplementary Figure VII. Effect of *MEOX2+Tcf15* and *CD36* on VLDL particle uptake.

Quantification of human APOB protein in cultured heart ECs overexpressing an empty vector or *MEOX2+Tcf15* (**A**) or in cultured *MEOX2+Tcf15* overexpressing heart ECs treated with *siRNA-NS* or *siRNA-CD36* (**B**) after incubation with human VLDL, revealing the occurrence of particle uptake but with no significant differences among the conditions tested (*n*=3).

Supplementary Figure VIII.
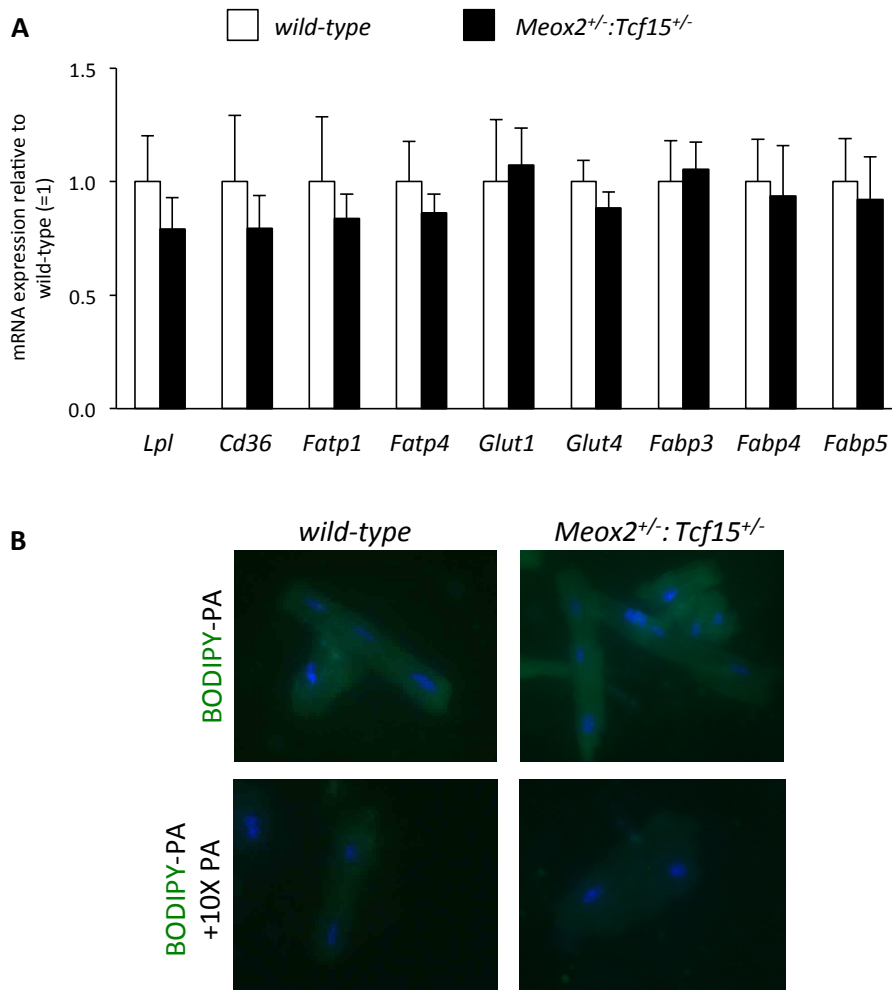
Supplementary Figure VIII. Effect of *Meox2+Tcf15* heterozygous deficiency on FA uptake in cardiomyocytes.

A, mRNA expression determined by qRT-PCR of genes encoding FA or glucose transport-related genes in cardiomyocytes freshly isolated from $Meox2^{+/-}:Tcf15^{+/-}$ littermates relative to wild-type cardiomyocytes (*n*=4) revealing no significant differences in expression. **B,** Representative fluorescence micrographs of cultured cardiomyocytes from wild-type or $Meox2^{+/-}:Tcf15^{+/-}$ littermates exposed to BODIPY-palmitic acid (PA; in green), counterstained with DAPI for nuclei (in blue), revealing no differences in PA uptake between genotypes. An excess (10X) of non-labeled PA was used as competition assay. Quantitative data represent mean ± s.e.m.

Supplementary Figure IX.
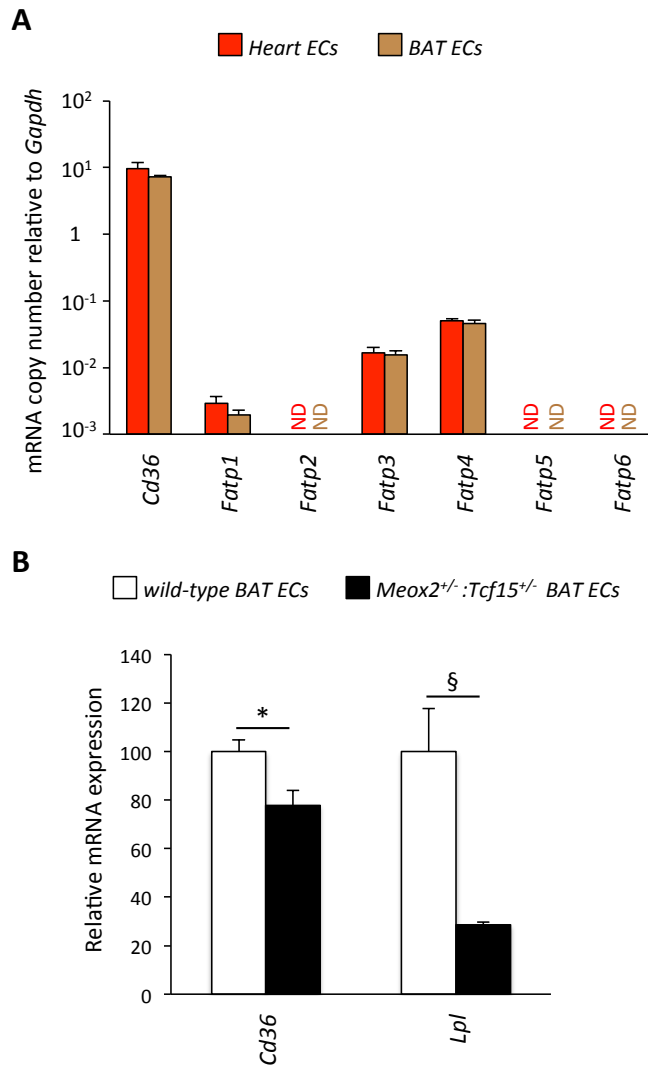
Supplementary Figure IX. Analysis of gene expression in BAT ECs.

A, Diagram representing qRT-PCR copy number quantification relative to *Gapdh* in murine heart ECs *versus* BAT ECs of the most described membrane FA translocase/transporters revealing no significant differences in expression. ND: not detectable. (n=4-7). **B,** Diagram representing qRT-PCR quantification of *Cd36* and *Lpl* in BAT ECs isolated from *Meox2$^{+/-}$:Tcf15$^{+/-}$* mice relative to wild-type littermates shown as representative genes regulated by Meox2/Tcf15 in heart ECs and also in BAT ECs (n=3-4; *$P<0.05$; $^{§}P$=0.056). Data represent mean ± s.e.m.

Supplementary Figure X.
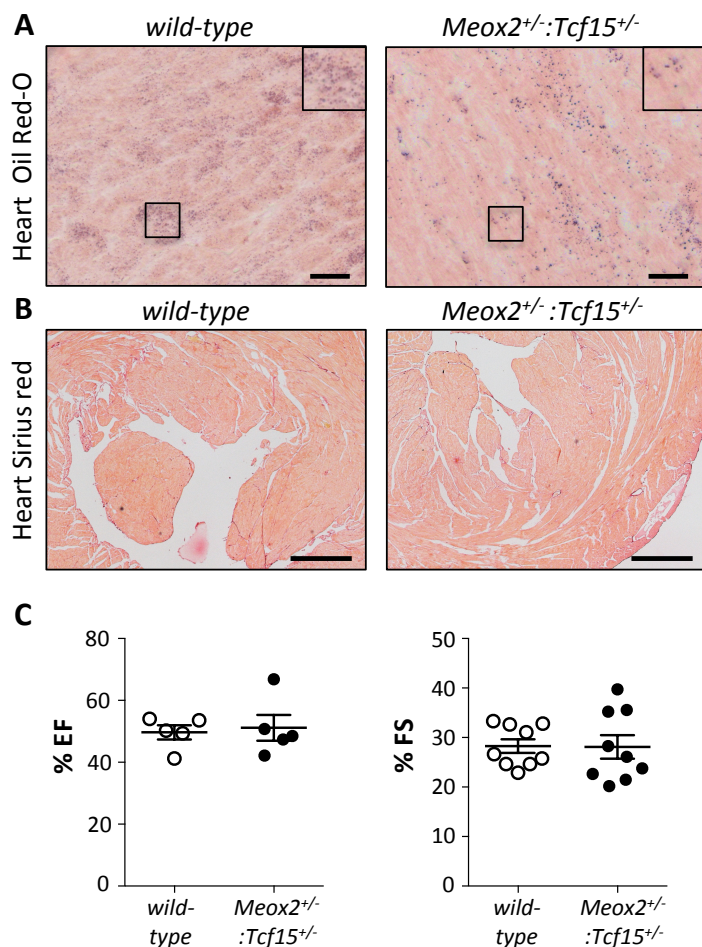
Supplementary Figure X. Young *Meox2$^{+/-}$:Tcf15$^{+/-}$* mice show reduced lipid storage but do not develop cardiac fibrosis or dysfunction.

A, Representative Oil Red-O (ORO)-stained cross-sections of wild-type or *Meox2$^{+/-}$:Tcf15$^{+/-}$* hearts Scale bars: 20 μm. **B,** Representative Sirius-red stained cross-sections of wild-type or *Meox2$^{+/-}$:Tcf15$^{+/-}$* hearts. Scale bars: 500 μm. **C,** Echocardiographic analysis of wild-type or *Meox2$^{+/-}$:Tcf15$^{+/-}$* mice showing % ejection fraction (% EF; *n*=5) and % fractional shortening (% FS; *n*=9). Quantitative data represent mean ± s.e.m.

III. SUPPLEMENTARY TABLES

Supplementary Table I. List of antibodies for FACS, magnetic bead sorting, Western blot, IF staining and GST pull-down assay.

Antigen	Species	Supplier, catalog N°	Label
CD31	Mouse	BD 558738	FITC
CD31	Mouse	BD 551262	APC
CD34	Mouse	BD 55138	PE
CD45	Mouse	BD 559864	APC
CD36	Mouse	Biolegend 102612	APC
CD31	Human	BD 555446	PE
CD31	Human	BD 555445	FITC
CD34	Human	BD 345804	APC
CD45	Human	BD 345808	FITC
PODOPLANIN	Human	Angiobio 11-009PE	PE
TIE2	Human	Reliatech 101-NBi54	Biotin
Endoglin	Mouse	R&D AF1320	None
Laminin	Mouse	Sigma L9393	None
Meox2	Mouse	Eurogentec	None
Tcf15	Mouse	Santa Cruz sc-46438	None
Gapdh	Human/Mouse	Cell Signaling 2118	None
α-Tubulin	Human/Mouse	Sigma T6199	None
ZDHCC2	Human	Santa Cruz sc-98219	None
RBP7	Human	Sigma HPA034749	None
BSI Lectin	Mouse	Sigma L3759	Biotin
FLAG	-	Sigma F1804	None
GST	-	Thermo scientific MA1-23238	None
CD31	Mouse	Biolegend 102502	None
CD102	Mouse	Biolegend 105602	None

Supplementary Table II. List of primers for qRT-PCR.

Gene	Species	Forward primer (5'3')	Reverse primer (5'3')
GAPDH	H	TGGTATCGTGGAAGGACTCATGAC	ATGCCAGTGAGCTTCCCGTTCAGC
ACTB	H	TGGCACCACACCTTCTACAATG	TAGCAACGTACATGGCTGGG
ABLIM3	H	CTTCATCACAGGCGAAGTCA	TTGGTCCACGAATCTTGATG
ADAMTS9	H	TACACCGCAAACGACTGTGT	TCACGATCGGGAGGTTTATC
ADH1	H	ATGGAGGTGTGGATTTTTCG	GTGCGTCCAGTCAGTAGCAG
AKAP5	H	GACGCCCTACGTTGATCTTT	CCAGGCATATTCATACCTTTCA
AQP7	H	GACTGGGGACACAGGGATAG	GGATGCTTGAACCATGTTTTG
C1QTNF9	H	AATGGTCTGCCTGGAAGAGA	CCTTTGATGCCTTTTGCTTC
CD36	H	CTGTCATTGGTGCTGTCCTG	TTGAATGTTGCTGCTGTTCA
EBF3	H	TGCCACCGTCATCATAATTG	TGCAGAACTGCTTGGATTTG
EEPD1	H	GTCACGACCTGACCCTTGTT	GGGTTCTTGGTGCTGATGTT
FAPB9	H	TGATGGGAAAATGATGACCA	CTCTTTGCCAAGCCATTTTT
H19	H	GAGCTCTCAGGAGGGAGGAT	CCAGCCTAAGGTGTTCAGGA
HN1I	H	TCCTTCCAGCAGGCCTAATA	CCAAAAATGTCGCTGGTCTT
KCNA5	H	CAGTTCCCCAACACACTCCT	CAGGGGCTTCTCCTCTTCTT
LPL	H	GTCCGTGGCTACCTGTCATT	TGTCCCACCAGTTTGGTGTA
MAP3K5	H	GCCCCTGCATGAAGAAATAG	TTAATGGACCCCATTTGGAA
MCTP1	H	TAATGCAGAAGTCCCCTTGG	CCACACAGGGTTGAGGTTCT
MEOX2	H	CCAGGAAAGAAAGGACAGCA	TCCACCCTTTACCCTCTTCC
MEOX2 UTR	H	TCTGGGACCACCTTCTTTTG	CCACCACCCTCTGTCACTTT
NAV3	H	GGACCGAGTGGTACTGGAAA	CAGAGAGCCCACATGATGAA
NTS	H	AAGCACATGTTCCCTCTTGG	AAGCCCTGCTGTGACAGATT
PAPSS2	H	GAGGTGGCTAAGCTGTTTGC	AAGCACACGCTCAGGAGTTT
PDPN	H	TGC TCT TCG TTT GG GAA GC	TCGCTGGTTCCTGGAGTCAC
PMP2	H	GGGGTTAGCCACCAGAAAAC	TCTCTTTGCCATCCCATCTC
PPARG	H	GACCACTCCCACTCCTTTGA	CGACATTCAATTGCCATGAG
PPARG UTR	H	CTCGAGGACACCGGAGAG	GGCTGACTCTCGTTTGAGAAA
PRND	H	ACCAAGGAGGCATTTGTCAC	GCTGCTGCACTCTGTACTGC
RBP7	H	TGCTGAAGCCACAGAAAGTG	AGGTGAGCCTGTCATTGTCC
RTN1	H	GAGTTTCCTGCTGCTGCTCT	AGGGTGATCTCAAGCTCCAA
SLC28A2	H	CCTTGGGGACATGACACTCT	GCTTTACCCCCTCCTCACTC
SLC27A1	H	GGTTCAGTACATCGGGGAGA	AGCAGCTCCATTGTGTCCTC
SLC27A3	H	TGTCCACCAGGAAGATGTGA	CCCCAATGTACTGGAACACC
SLC27A4	H	GGCTAAACCCTGCTGAGACC	AGCACCAGCTTGGAGAACAG
TCF15	H	GCAGCTGCTTGAAGGTGAG	CGGTCCCTACACAAAGAAGG
TCF15 UTR	H	TCCTGGAGAGCTGTGAGGAT	CCCAGAACATCTGTGCCTCT
TIMP4	H	CAGACCCTGCTGACACTGAA	AGACTTTCCCTCTGCACCAA
WT1	H	CAAATGACATCCCAGCTTGA	GACACCGTGCGTGTGTATTC
WT1 UTR	H	CAGGCTGCTAACCTGGAAAG	CTCCATTTGTGCAAGGAGGT

ZDHHC2	H	TTGCGGCAACAGATTTACAG	TGCTGACTAGCCAACAATGA
ACTA2	H	TGGTGTGTGACAATGGCTCT	CTTTTCCATGTCGTCCCAGT
PROX1	H	CAGTACTGAAGAGCTGTCTATAACCAGAG	TCTGAGCAACTTCCAGGAATCTC
PTPRC	H	GACAACAGTGGAGAAAGGACG	GGGAAGGTGTTGGGCTTTG
TIE2	H	ACACCTGCCTCATGCTCAGC	AGCAGTACAGAGATGGTTGCATTC
PECAM1	H	TCTGCACTGCAGGTATTGACAA	CTGATCGATTCGCAACGGA
Tubb	M	GGGAGGTGATAAGCGATGAA	CCCAGGTTCTAGATCCACCA
Gapdh	M	CCGCATCTTCTTGTGCAGT	GAATTTGCCGTGAGTGGAGT
Actb	M	GACGGCCAGGTCATCACTAT	CTTCTGCATCCTGTCAGCAA
Ablim3	M	CAGTCACTTCTGGCACTGGA	CCCCTCAGTGAACATCTGGT
Actc1	M	CAGCTGCATCTTCCTCCTCT	ATGGTGGTGCCTCCAGATAG
Adamst9	M	ACCCGGATGAGATACGTCAG	GGTCAGTCTCGGGGATGTAA
Adh1	M	ACAAACCCTTCACCATCGAG	CCTTCTCCAACGCTCTCAAC
Airn	M	CGGCAGTTTGGTTTACAGGT	CTGGTGTCCCTGTTGGTTCT
Akap5	M	AGCAGAGCTGGCCAGAGAC	TGTGACTTCTTCAGGACACGA
Akr1c19	M	AGCTCTAGAGGCTGGGTTCC	CAGCTCTGGCCTATGGAAAG
Aqp7	M	CTCGGTGTCAACTTGGGTTT	CCTTGGAACCTGTCACCAAC
C1qtnf9	M	AGGTCACAATGGCCTACCTG	AGCCTGGATCACCTTTGATG
Cox8b	M	TGCGAAGTTCACAGTGGTTC	TGCTGCGGAGCTCTTTTTAT
Dmtp	M	CAATGGAACTACGCCTGCAT	AATATGGGCACCTCTTGCTG
Ebf3	M	CTCGACACATCCCTGGAGTT	GTAACCTTTCGGGGTCACCT
Eepd1	M	TTTGGAGGTATGAGGGATGG	GCCTCTTTGTCAAGCAGCTC
Enpp3	M	CAGCTACGGGAACAATGGAT	CCTCTGTGCGATGAGTCAAA
Fabp3	M	GACGAGGTGACAGCAGATGA	TGCCATGAGTGAGAGTCAGG
Fabp9	M	ATGGACATCCAAGCAGGAAG	CTGTTTGCCAAGCCATTTTT
Gda	M	GTGGTGCTTCAAACCATGTG	TTCTTCAGCCACATCAGTGC
H19	M	AATGGTGCTACCCAGCTCAT	GCAGAGTTGGCCATGAAGAT
Hn1l	M	AGGCAAAGGAAGTGGGATCT	TGGAGGATTTGTCCTCTTGG
Kcna5	M	CGCTACTTCGATCCCTTGAG	CAGCTGGTAAAAGCGGATCT
Klra10	M	GGCCAAGCAATGAACTTCTG	ATGCTGGCAGTTCGCTTTAC
Klra9	M	AGATTCCTCACGGGACACAG	ATTGGCCATTGTCAATCCAT
Lamb1	M	GGAACCGGAGTTCAGCTATG	GGGTTGAGGGTCTCGTGATA
Lipg	M	ACCTACACGCTGTCCTTTGG	GCTGAGGCAGATTCCCCTTT
Lpl	M	TTTGGCTCCAGAGTTTGACC	GTCTTGCTGCTGTGGTTGAA
Map3k5	M	GGCCAACAACATCATCCTCT	GCCACCTTCAAAAGCTGAAC
Mb	M	CACCCTGAGACCCTGGATAA	GAGCATCTGCTCCAAAGTCC
Mctp1	M	CAGTAATGCAGATGTCCCTTTG	CAAGAAAGGCTGAGCCCATA
Meox2	M	GGCAGAATTTGCCCATCATA	TGCTCAGAGCTGTGGTCACT
Myh6	M	CCACCCAAGTTCGACAAGAT	AGGCGTTGTCAGAGATGGAG
Myl2	M	GACCCAGATCCAGGAGTTCA	TCAGCCTTCAGTGACCCTTT
Myl3	M	AAGGGCGAGATGAAGATCAC	GCAGGAACGTCTCAAAATCC

Myoz2	M	CCATGCAGAATGGGAGAGTT	TTTGGGTACAAAGCCTCCAG
Nav3	M	AAGCAAGCAGTGACCTGGAT	AGGGGACAGTGATGTTGGAG
Nts	M	TTCACAATGAGTTGCCAGGA	GTGTGGACCTGCTTGTCAGA
Papss2	M	GTCTACCAGGCCCATCATGT	GACATTGTCCCCATCCAGAG
Pmp2	M	GTGGGGTTAGCCAACAGAAA	TCTCCAGTGTCACGATGCTC
Pparg	M	CAGGCCTCATGAAGAACCTT	GGATCCGGCAGTTAAGATCA
Prg4	M	GCCACCTGCAACTGTGATTA	CTGCACAGCACTTGCCATAC
Prnd	M	CTGGGTTTCGTTTGGTTCAT	CCCTGGCAGATACTCCGTTT
Rbp7	M	TCAGCGGTACCTGGAATCTT	AGGCTCGTGCATTTTCTGTT
Rtn1	M	CATCAGCTTCCGCATCTACA	AAAGCCTCCGTAGCTCCTTC
Slc28a2	M	GAGCAGCTGATCTCCTTTGC	ATCTGATCTCCCAGCCATTG
Tcf15	M	GCTCCATCTGCACCTTCTGT	TTGTCCTCCGGTCCTTACAC
Timp4	M	ACACGCCATTTGACTCTTCC	CAGCCACAGTTCTGGTGGTA
Tnnc1	M	CAGCAAAGGGAAGTCTGAGG	CGTGCAAGACCAGCATCTAC
Tnni3	M	GAAGCAGGAGATGGAACGAG	TGACTTTTGCTTCCACGTCA
Tnnt2	M	CTGAGACAGAGGAGGCCAAC	TTCTCGAAGTGAGCCTCGAT
Wt1	M	AGGTTTTCTCGCTCAGACCA	GCTGAAGGGCTTTTCACTTG
Zdhhc2	M	GCTGTACTGCCTTTTCATTGC	CCAAACAGAGAGGACAAGCTG
Acta2	M	CGCTGTCAGGAACCCTGAGA	CGAAGCCGGCCTTACAGA
Ptprc	M	GCCCCGGGATGAGACAGT	TTTGAAAGCCCGAGTGCCT
Cdh5	M	ATTGAGACAGACCCCAAACG	TTCTGGTTTTCTGGCAGCTT
Ng2	M	CCTTCCTACAAGTGACCATTGC	CCTGAATTCACTGCCTCCTG
Pdpn	M	GCCAGTGTTGTTCTGGGTTT	AGAGGTGCCTTGCCAGTAGA
Pecam1	M	GTCATGGCCATGGTCGAGTA	CTCCTCGGCGATCTTGCTGAA
Prox1	M	CGCGTGGGTTTCTTCTCTGC	GGGCTGTGCTGTCATGGTCA
Tek	M	GAAACATCCCTCACCTGCAT	TGGCCTTTTCTCTCTTCCAA
Fabp5	M	CAAAACCGAGAGCACAGTGA	CCCTCATTGCACCTTCTCAT
Slc2a4	M	ATTCTGGTTGCC CAGGTGCT	ATTGGACGCTCTCTCTCCAA
Slc2a1	M	CCGCCTCATGTTGGCTGT	TGTGGTGGATGGGATGGG
Gpihbp1	M	GGGCACAAGAAGATGGTGAT	CTGGAGCAGCTCTGTGTCTG
Slc27a1	M	ACCACTCTGCAGGGAACATC	AGCGGCAGATTTCACCTATG
Slc27a2	M	ATGCCGTGTCCGTCTTTTAC	TAGCAAGGCCTGTCCCATAC
Slc27a3	M	AGGCTGCTCGAATCAGTCAT	AACTTGGGTTTCAGCACCAC
Slc27a4	M	CTACCCAAAGCTGCCATTGT	GAACTTCTTCCGGATCACCA
Slc27a5	M	TCGGATCTGGGAATTCTACG	CAGGAATGCAAAAACCCTGT
Slc27a6	M	ACGTCAGAGTTTGGGGAATG	TGCAACTGGCTAATCACAGC
CD36	M	TGCCAGTCGGAGACATGCT	GCCACGTCATCTGGGTTTTG
Fabp4	M	TGGAAGCTTGTCTCCAGTGA	TCGACTTTCCATCCCACTTC
Flt1	M	TGGCCAGAGGCATGGAGT	TCGCAAATCTTCACCACATGG
Nrp1	M	ACACCTGAGCTTCGGACGTT	CCACTGTGTGTGGCTCTCTCA

H: human; M: mouse

Supplementary Table III. Cardiomyocyte size and capillary counts in young and aged wild-type and *Meox2$^{+/-}$:Tcf15$^{+/-}$* mice.

	Cardiomyocyte size (μm^2)	Capillary count (N°/N° cardiomyocytes)
wild-type (young)	351 ± 17	0.99 ± 0.07
***Meox2$^{+/-}$:Tcf15$^{+/-}$* (young)**	369 ± 29	0.97 ± 0.08
***P*-value**	0.59	0.85
wild-type (aged)	298 ± 23	0.78 ± 0.01
***Meox2$^{+/-}$:Tcf15$^{+/-}$* (aged)**	345 ± 28	0.69 ± 0.02*
***P*-value**	0.21	0.005

Data represent mean ± s.e.m. (*n*=4 for young; *n*=7 for aged; *P<0.05 *versus* wild-type).

Supplementary Table IV. Echocardiographic parameters in 11 month-old wild-type and *Meox2$^{+/-}$:Tcf15$^{+/-}$* males.

	IVSd/BSA (mm/cm^2)	PWd/BSA (mm/cm^2)	LVIDd/BSA (mm/cm^2)	LVIDs/BSA (mm/cm^2)	EF (%)	FS (%)	HR (bpm)
wild-type	0.57±0.03	0.57±0.03	3.9±0.1	2.6±0.1	59.9±3.5	33.2±3.0	500±25
Meox2$^{+/-}$:Tcf15$^{+/-}$	0.56±0.03	0.50±0.05	4.1±0.2	3.2±0.2	45.2±4.8	22.8±3.6	501±22
***% Meox2$^{+/-}$:Tcf15$^{+/-}$ versus* wild-type**	98±6	88±8	106±4	123±9*	75±8*	68±11*	100±4
***P*-value**	0.85	0.26	0.31	0.04	0.03	0.04	0.98

Abbreviations: IVSd: interventricular septal thickness at end-diastole; BSA: body surface area; PWd: posterior wall thickness at end-diastole; LVIDd: left ventricular internal diastolic diameter; LVIDs: left ventricular internal systolic diameter; EF: ejection fraction; FS: fractional shortening; HR: heart rate; bpm: beats per minute. Data represent mean ± s.e.m. (*n*=8-9; *P<0.05; *versus* wild-type).

IV. SUPPLEMENTAL REFERENCES

1.   Motoike T, Loughna S, Perens E, Roman BL, Liao W, Chau TC, Richardson CD, Kawate T, Kuno J, Weinstein BM, Stainier DY, Sato TN. Universal gfp reporter for the study of vascular development. *Genesis*. 2000;28:75-81

2.   Burgess R, Rawls A, Brown D, Bradley A, Olson EN. Requirement of the paraxis gene for somite formation and musculoskeletal patterning. *Nature*. 1996;384:570-573

3.   Aranguren XL, Agirre X, Beerens M, Coppiello G, Uriz M, Vandersmissen I, Benkheil M, Panadero J, Aguado N, Pascual-Montano A, Segura V, Prosper F, Luttun A. Unraveling a novel transcription factor code determining the human arterial-specific endothelial cell signature. *Blood*. 2013;122:3982-3992

4.   Aranguren XL, Beerens M, Coppiello G, Wiese C, Vandersmissen I, Lo Nigro A, Verfaillie CM, Gessler M, Luttun A. COUP-TFII orchestrates venous and lymphatic endothelial identity by homo- or hetero-dimerisation with PROX1. *J Cell Sci*. 2013;126:1164-1175

5.   Hendrickx B, Verdonck K, Van den Berge S, Dickens S, Eriksson E, Vranckx JJ, Luttun A. Integration of blood outgrowth endothelial cells in dermal fibroblast sheets promotes full thickness wound healing. *Stem Cells*. 2010;28:1165-1177

6.   Koopman R, Schaart G, Hesselink MK. Optimisation of Oil red O staining permits combination with immunofluorescence and automated quantification of lipids. *Histochem Cell Biol*. 2001;116:63-68

7.   Chi JT, Chang HY, Haraldsen G, Jahnsen FL, Troyanskaya OG, Chang DS, Wang Z, Rockson SG, van de Rijn M, Botstein D, Brown PO. Endothelial cell diversity revealed by global expression profiling. *Proc Natl Acad Sci U S A*. 2003;100:10623-10628

8.   Greenwalt DE, Scheck SH, Rhinehart-Jones T. Heart CD36 expression is increased in murine models of diabetes and in mice fed a high fat diet. *J Clin Invest*. 1995;96:1382-1388

9.   Yang L, Han Y, Suarez Saiz F, Minden MD. A tumor suppressor and oncogene: The Wt1 story. *Leukemia*. 2007;21:868-876

10.   Abbott NJ, Patabendige AA, Dolman DE, Yusof SR, Begley DJ. Structure and function of the blood-brain barrier. *Neurobiol Dis*. 2010;37:13-25

11.   Geraud C, Schledzewski K, Demory A, Klein D, Kaus M, Peyre F, Sticht C, Evdokimov K, Lu S, Schmieder A, Goerdt S. Liver sinusoidal endothelium: A microenvironment-dependent differentiation program in rat including the novel junctional protein liver endothelial differentiation-associated protein-1. *Hepatology*. 2010;52:313-326

12.   Caprioli A, Zhu H, Sato TN. CRBP-III:Lacz expression pattern reveals a novel heterogeneity of vascular endothelial cells. *Genesis*. 2004;40:139-145

13.   Skowronski MT, Lebeck J, Rojek A, Praetorius J, Fuchtbauer EM, Frokiaer J, Nielsen S. Aqp7 is localized in capillaries of adipose tissue, cardiac and striated muscle: Implications in glycerol metabolism. *Am J Physiol Renal Physiol*. 2007;292:F956-965

14.   Zizola CF, Schwartz GJ, Vogel S. Cellular retinol-binding protein type III is a PPARgamma target gene and plays a role in lipid metabolism. *Am J Physiol Endocrinol Metab*. 2008;295:E1358-1368

15.   Kishida K, Shimomura I, Nishizawa H, Maeda N, Kuriyama H, Kondo H, Matsuda M, Nagaretani H, Ouchi N, Hotta K, Kihara S, Kadowaki T, Funahashi T, Matsuzawa Y. Enhancement of the aquaporin adipose gene expression by a peroxisome proliferator-activated receptor gamma. *J Biol Chem*. 2001;276:48572-48579

Giulia Coppiello, Maria Collantes, María Salomé Sirerol-Piquer, Sara Vandenwijngaert, Sandra Schoors, Melissa Swinnen, Ine Vandersmissen, Paul Herijgers, Baki Topal, Johannes van Loon, Jan Goffin, Felipe Prósper, Peter Carmeliet, Jose Manuel García-Verdugo, Stefan Janssens, Iván Peñuelas, Xabier L. Aranguren and Aernout Luttun

The online version of this article, along with updated information and services, is located on the
World Wide Web at:
http://circ.ahajournals.org/content/131/9/815
Free via Open Access

Data Supplement (unedited) at:
http://circ.ahajournals.org/content/suppl/2015/01/05/CIRCULATIONAHA.114.013721.DC1.html